crystals

MDPI

Review

Recent Developments on Relaxor-$PbTiO_3$ Ferroelectric Crystals

Lkhagvasuren Baasandorj [1,*] and Zibin Chen [2]

[1] Institute for Superconducting and Electronic Materials, Australian Institute of Innovative Materials, University of Wollongong, Wollongong, NSW 2500, Australia
[2] Department of Industrial Systems Engineering, The Hong Kong Polytechnic University, Hung Hom, Hong Kong, China; zi-bin.chen@polyu.edu.hk
* Correspondence: lb634@uowmail.edu.au

Abstract: Numerous investigations on the development of the relaxor-$PbTiO_3$ ferroelectric crystals have been carried out since their extraordinary properties were revealed. Recent developments on these crystals have offered further advances in electromechanical applications. In this review, recent developments on relaxor-$PbTiO_3$ crystals and their practical applications are reviewed. The single crystal growth methods are first discussed. Two different strategies, poling and doping, for piezoelectric improvement are surveyed in the following section. After this, the anisotropic features of the single crystals are discussed. Application perspectives arising from the property improvements for electromechanical devices are finally reviewed.

Keywords: ferroelectric single crystals; relaxor-PT; doping; poling; anisotropy; electromechanical applications

Citation: Baasandorj, L.; Chen, Z. Recent Developments on Relaxor-$PbTiO_3$ Ferroelectric Crystals. *Crystals* **2022**, *12*, 56. https://doi.org/10.3390/cryst12010056

Academic Editors: Serguei Petrovich Palto and Marek Szafrański

Received: 22 November 2021
Accepted: 27 December 2021
Published: 31 December 2021

Publisher's Note: MDPI stays neutral with regard to jurisdictional claims in published maps and institutional affiliations.

1. Introduction

Extraordinary properties of relaxor-$PbTiO_3$ (PT) ferroelectric crystals have outperformed those of the state-of-the-art piezoelectric $Pb(Zr,Ti)O_3$ (PZT) ceramics [1–5]. The unique properties of relaxor-PT crystals have hence brought significant improvements to diverse electromechanical applications, including medical transducers, actuators and sensors [1,2]. The chronological development of relaxor-PT single crystals consists of three generations. The first generation is the class of binary $Pb(Zn_{1/3}Nb_{2/3})O_3$-$PbTiO_3$ (PZN-PT) and $Pb(Mg_{1/3}Nb_{2/3})O_3$-$PbTiO_3$ (PMN-PT) single crystals, which show ultra-high electromechanical and piezoelectric properties [5–10]. The second generation includes $Pb(In_{1/2}Nb_{1/2})O_3$-$Pb(Mg_{1/3}Nb_{2/3})O_3$-$PbTiO_3$ (PIN-PMN-PT) crystals demonstrating a greater coercive field (E_C) and a higher rhombohedral-to-tetragonal phase transition temperature ($T_{r\text{-}t}$) and a higher Curie temperature (T_C) [11–16]. The third generation is Mn-modified $Pb(In_{1/2}Nb_{1/2})O_3$-$Pb(Mg_{1/3}Nb_{2/3})O_3$-$PbTiO_3$ (Mn:PIN-PMN-PT), which features a large mechanical quality factor (Q_m) meanwhile retains comparable piezoelectric properties to earlier generations [17,18]. Figure 1 exhibits comparison on composition dependent property of three generation crystals including PMN-PT, PIN-PMN-PT and Mn:PIN-PMN-PT.

Since discoveries of relaxor-PT ferroelectric crystals, immense attention has been paid to explain the unique behavior and advancing properties in these interesting materials. Various strategies for property improvements have been studied. Among them, the fabrication with morphtropic phase boundary (MPB) is a conventional way of bringing enhancements, but it has been shown to reach a plateau [1,4,19,20]. Poling strategy still attracts attentions, and in particular, alternating current (electric-field) poling (ACP) has been recently confirmed to bring drastic increases in piezoelectric and electromechanical properties in relaxor-PT crystals [5,21–23]. Such improvements offer further advances in electromechanical technologies. The doping strategy still retains its intensive potential for purpose-oriented property improvement. For Pb-based piezoelectric materials, the effects

of "accepter" and "donor" dopings have been intensively investigated [17,18,20,24]. The doped relaxor-PT single crystals have been proved to demonstrate significant advances for devices applications [2]. In addition, the anisotropic features of the relaxor-PT single crystals are crucial for various designs of devices [1–7].

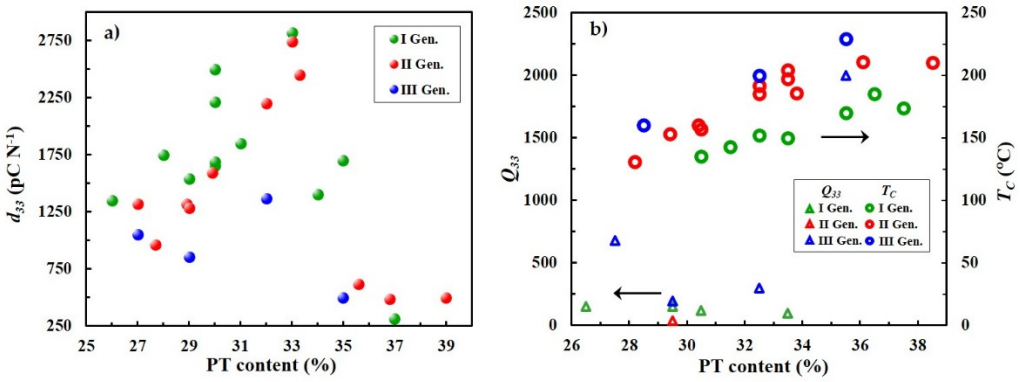

Figure 1. Property comparisons between three generation crystals (PMN-PT, PIN-PMN-PT and Mn:PIN-PMN-PT). (**a**) longitudinal piezoelectric coefficient. (**b**) longitudinal mechanical quality factor and the Curie temperature. Data from refs. [15,23,25–42].

This review surveys the recent progress on the properties of relaxor-PT crystals and offers perspectives on their practical significance. Firstly, two crystal growth methods, the modified Bridgman method and solid-state conversion growth method, and their progress are discussed in Section 2. The next section discusses piezoelectric and electromechanical improvement strategies, including poling procedure and doping approach. The poling strategy consists of DC and AC poling techniques. Doping-induced property enhancements are covered in Section 3.2. These enhancements are achieved by either donor doping or acceptor doping depending on different requirements such as higher piezoelectricity or increasing mechanical quality factor. Anisotropic features of their piezoelectric and electromechanical properties are reviewed in Section 4. In the final section, recent progress on electromechanical applications based on the unique properties of relaxor-PT crystals is reviewed, including the most recent reports and perspectives for applications.

2. Single Crystal Growth

Relaxor-PT single crystals are synthesized by different methods, including conventional flux growth, flux Bridgman growth, modified Bridgman growth, and solid-state conversion growth. This section highlights two growth methods: modified Bridgman growth and solid-state conversion growth. These two growth methods are suitable for the fabrication of single crystals with high quality on an industrial scale.

2.1. The Modified Bridgman Method

P.W. Bridgman invented a simple and straightforward growth technique for single crystal in the 1920s [43]. Since then, several modifications have been developed for this method. In the 1930s, D. C. Stockbarger introduced a sophisticated modification that became fundamental to the modern Bridgman method [44].

By using this method, large, high-quality relaxor-PT single crystals can be grown [6,14,25,45–50]. Figure 2 shows an as-grown boule of Mn-doped PIN-PMN-PT single crystal. The material is melted at a higher temperature than its melting point. Then, it is slowly transported into a lower temperature zone. During the transport, the melt is gradually crystallized through the temperature gradient and solidus line of the solid solution phase diagram [43,45]. Prior to the crystal growth, it is necessary to pre-synthesize $MgNb_2O_6$ to avoid achieving parasitic-pyrochlore phase, using the two-step Columbite precursor method [26]. The sintered ceramic sample is introduced into an ultrapure platinum crucible. The high purity of the crucible prevents any reaction between the melting

materials and the platinum [45]. The platinum crucible is sealed, and then placed in a cylindrical alumina crucible. The space between the two crucibles is filled with alumina sand for the purposes of supporting the Pt crucible and absorption of any volatiles. The alumina crucible is then placed on a ceramic tube that is part of the translation system. The furnace used in Bridgman growth method consists of two zones. Zone I provides high temperature where the material is melted. In zone II, there is lower temperature given for generation of temperature gradient between the two zones while the charge is being moved. After the material is melted, the ingot is dwelled for a certain period. Then, the translation system moves the charge down to zone II with a speed that is slower than that of the material's crystallization [45,47]. The temperature of the crystallization process is monitored by several thermocouples. Single crystals can be grown along the major crystallographic orientations of <111>, <110> and <001>. To control the growth orientation, an orientated single-crystal seed is used [46,47].

Figure 2. As-grown boule of Mn-modified PIN-PMN-PT single crystal.

Shimanuki et al. grew the first relaxor-PT single crystal using the vertical Bridgman method. In their experiment, the charge was suspended inside the furnace, and it was then moved down to the lower zone to be crystallized [7]. Luo et al. used the modified Bridgman method to grow PMN-PT single crystals [6]. Instead of the suspension technique, an automatic up-down mechanism was used to control the charge movement, a platinum crucible was shaped to a tapered end enabling a single grain growth, and the crucible was also sealed with a lid that protected the contents from volatiles at high temperature. The melting point was chosen based on thermogravimetric measurements. The properties of the single crystal are: piezoelectric charge coefficient, d_{33} > 2000 pC/N, dielectric constant, ε~5500, and electromechanical coupling factor, k_{33}~93% at the MPB [6,48]. Using the modified Bridgman method, it was grown the ternary PIN-PMN-PT single crystals and the materials showed comparable piezoelectric and electromechanical responses to that of their binary PMN-PT counterparts but with higher Curie temperature and coercive field [14,25].

Composition segregation is an unavoidable disadvantage of the Bridgman method for growing solid solution crystals. Figure 3 shows the segregation of Ti^{4+} ion and longitudinal piezoelectric variation along growth direction with three different modified Bridgman methods. Because of different melting points and various densities of the composition members, this method is unavoidably producing inhomogeneous products. Ti^{4+} cation is the most segregated ion while Pb^{2+} cation is relatively homogeneous along the growth axis of the as-grown boule. This segregation leads to property variation and cost increase [14,26–30,45,46,50]. It is found that property homogeneity is stable in the radial direction but varies along the growth direction [47]. To avoid compositional variation, Zawilski et al. used the vertical zone levelling technique, resulting in homogeneous Ti^{4+} content over a 60 mm length along the growth direction [51].

Rare-earth doped PMN-PT single crystal also showed a reduced property variation along the growth direction. In Sm-doped PMN-PT single crystals, Sm^{3+} and Ti^{4+} cations favour the tetragonal phase but the segregation of these two cations show opposite trend, and as a result, property homogeneity is expanded [24].

The continuous feeding Bridgman method (CFBG) is an advanced modified method with advantages for addressing size and segregation issues. During the crystallization, pre-synthesized material of the same composition is continuously introduced into the melt to enlarge the final boule. This modification also provides uniform distributions of the 0.70PMN–0.30PT, 0.24PIN–0.46PMN–0.30PT and 0.31PIN–0.43PMN–0.26PT compositions along the axis direction [52–54]. The PMN-PT single crystal with 80 mm in diameter and 320 mm in length was grown with this method, and variations of d_{33} and Ti^{4+} segregation were within 10% and 6% along the growth direction, respectively [52]. In the case of a PIN-PMN-PT single crystal, the property variation and Ti^{4+} segregation were reduced to 15% and 6%, respectively, over the axis length of the as-grown boule [54].

The multi-crucible configuration is another modified Bridgman method for both reducing cost and increasing mass production [45,55,56]. In this modified method, the high-temperature furnace has five chambers, each of which comprises three zones: upper, hot, and lower. Using this configuration, Han et al. grew PMN-PT crystals with 75 mm in diameter [45]. In the case of PIN-PMN-PT crystal, the size of the grown crystal was 101.6 mm in diameter and 100 mm in length [55].

The Bridgman growth method is a consistent way of growing large, high-quality single crystals. This method has the disadvantage of compositional non-uniformity. There have recently been several advances on this issue, however, including doping, continuous feeding, and multi-furnace growth. These advances enable the production of large crystals with low cost and a higher grade for commercial needs.

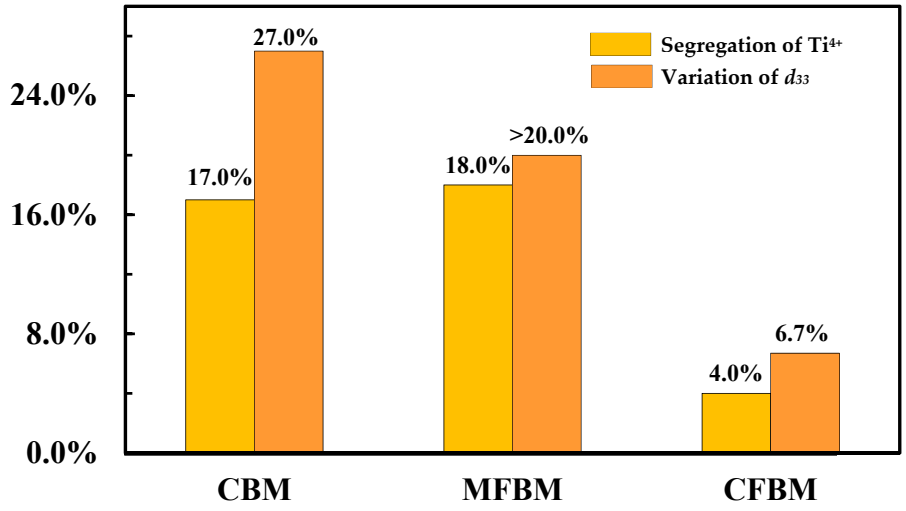

Figure 3. Compositional segregation and d_{33} variation along growth direction of the PIN-PMN-PT boules grown by different modified techniques: conventional Bridgman method (CBM-left), multi-furnace Bridgman method (MFBM-middle) and continuous-feeding Bridgman method (CFBM-right). Data from refs. [50,54,55].

2.2. Solid-State Conversion Growth Method

In the modified Bridgman methods, cost and operational complications remain unsolved. The flux method for the growth of single crystals is an alternative way for simple operation and fabricating homogenous single crystals. However, its small quantity of output is inconvenient for mass production.

The solid-state conversion growth (SSCG) method has appreciable advantages with respect to cost and operational complications over the melt growth methods. This method could produce cost-efficient, homogeneous, and large single crystals. The operation for crystal growth is also simpler compared to the melt growth methods. Table 1 demonstrates a comparison between Bridgman method and SSCG method.

Table 1. Comparison between Bridgman method and SSCG method.

	BM	SSCG
Cost	High	Medium
Complexity of operation	High	Medium
Homogeneity of product	Low	High
Porosity of product	Low	High
Quantity of product	Large	Large
Progress in issue	Successful	Successful

In polycrystalline materials, grains grow in two major ways: normal grain growth and non-normal grain growth. In the real system, non-normal grain growth occurs, and different models for it have been proposed. Abnormal grain growth (AGG) is a type of non-normal grain growth, [57–59]. In AGG, the grains grow via either atomic diffusion or interface reaction, depending on the driving force for migration of boundary. In AGG, faceted boundary migration is dominant [60,61]. By applying the grain growth mechanism, a polycrystalline material could be converted into a single crystal [57,62–66]. In the polycrystalline-single crystal conversion process, a single crystal seed is used to nucleate the AGG. Here, the seed could act as a large AGG grain that consumes the fine grains of the matrix to further grow the single crystal. As shown in Figure 4, the seed with preferred orientation could be either embedded or bonded in the matrix, depending on the characteristics of the particular material. Afterwards, the sample is annealed at a high temperature but below the melting point. This method is therefore useful for materials that have a high melting point and easy volatility. The most important aspect of the conversion method is controlling the microstructure [60,67]. Generally, a non-uniform grain-size distribution of the matrix entails AGG grains in a matrix. When the matrix AGG grains are nucleated, they impinge on the newly grown single crystal and restrict its growth. It is therefore crucial to provide fine grains in the matrix. To control the grains in the matrix, dopants are used to inhibit AGG of the matrix. Li_2O dopant, for instance, reduces the critical driving force of grain growth, and leads to small grains [68]. Porosity is the main drawback of the SSCG method. Pores degrade the physical properties of single crystals. Various attempts have been studied to reduce the porosity, where adding a dopant is one of the ways [69]. Choosing an <001>-oriented seed is another way because the low speed of growth leads to minimum porosity and this orientation provides the slowest growth rate compared to the <111> and <110> orientations [70]. Changing the atmosphere, such as the oxygen pressure for sintering, could also reduce pores [68]. Of particular importance is that hot-pressing of the ceramic matrix will positively reduce porosity in the as-grown crystal [11,31,68].

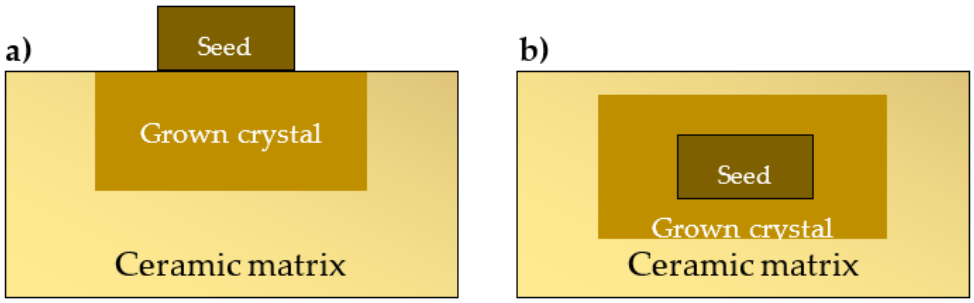

Figure 4. Crystal growth from seed into a ceramic matrix. (**a**) templated growth and (**b**) embedded growth.

Relaxor-PT crystals, including PMN-PT and $Pb(Mg_{1/3}Nb_{2/3})O_3$–$PbZrO_3$–$PbTiO_3$ (PMN-PZ-PT) single crystals, were successfully grown by the SSCG method. A certain excess of PbO was added to increase the kinetics of growth. This is because the liquid phase of PbO wets the grain boundaries during the sintering [68,70–72]. For relaxor-PT single crystal growth, the seed is chosen with regard to growth kinetics [70,72], stability [11,31],

and lattice matching [68]. The properties of early single crystals grown by SSCG were inferior to those grown by the melt growth methods. Due to the successful attempts to overcome the porosity issue, however, the relaxor-PT single crystals grown by the SSCG method produced quite similar piezoelectric and electromechanical responses to those grown by the melt methods [11,31]. In addition, since the SSCG method has demonstrated that it could produce large size commercial products with high piezoelectric performance, this technique is able to directly grow specifically designed crystals for a particular application [57,61], leading to savings in time and cost.

3. Property Improvements

Achievement of the MPB composition in solid solution Pb-based ferroelectric materials has been a traditional strategy in the last several decades to reach the highest dielectric and piezoelectric responses [1,5,19,73]. Nonetheless, this strategy was shown to reach a plateau where no further enhancement could be expected. In addition to the MPB, the local structure heterogeneity inherently associated with the randomly located B-site cations of the relaxor-PT ferroelectrics also contributes greatly to the properties [74].

Strategies depending on poling and doping have been actively studied in the last several years, and proved to be very effective to enhance the principal properties of relaxor-PT ferroelectric crystals. This section will investigate the current advantages of both poling and doping methods.

3.1. Poling Strategy

Applying an external field enables us to control the ferroelectric/ferroelastic domains and to use the related properties for practical demands. Producing desirable domain configurations is thus of both scientific and technological interest [75]. Poling techniques for relaxor-PT crystals, including traditional direct current (electric-field) poling (DCP) [1,5,19] and alternating current (electric-field) poling (ACP), have recently attracting a lot of attention [23].

3.1.1. DCP

DCP is a traditional technique used to align the polarization of ferroelectric materials, thus exhibiting piezoelectricity. In relaxor-PT single crystals, the poling along nonpolar direction will lead to engineered domain configurations, accounting for the high piezoelectricity observed in single crystals when compared to their ceramic counterparts. The effects of field strength and the influence of temperature are always of interest in maximizing material properties [2].

Threshold DC Field and Over-Poling Effect

To reveal the maximum piezoelectric property in a ferroelectric material, a low DC field is not sufficient for full polarization. However, a field that is too high could over-polarize the material and degrade its properties. It is thus crucial to find an appropriate field range for an efficient poling procedure [76]. The DC electric field effect on the properties of relaxor-PT crystals has been intensively studied [32,77–90]. In general, the longitudinal piezoelectric coefficient in PMN-PT single crystal is raised under a moderate DC-field at room temperature. The highest order of d_{33} is found in the MPB composition, where polar rotation exists from rhombohedral to monoclinic (M_A) phase [81,82,91–93]. For the 0.70PMN-0.30PT composition, M_A phase is induced starting from a~2.0 kV/cm field (with its coercive field 2.2–2.5 kV/cm). The maximum value of d_{33} is reached at ~4.0–6.0 kV/cm [79–81,84]. In order to achieve a sufficiently poled sample, an electric field at 2–3 times the coercive field (E_C) is applied in practice. After continuously increasing the electric field, the over-poling effect takes place, and the piezoelectric coefficient decreases, owing to the stability of the new electric field-induced phase [80,82], vulnerability to sample cracking [94], and the tetragonal phase transition [75,95,96]. It is important to note that the

magnitudes of electric fields are varied in different compositions of crystals because of the coercive field difference.

In order to avoid degrading the piezoelectric property during the poling process, it is always important to find the threshold of the over-poling field for practical applications of relaxor-PT single crystals.

High-Temperature DCP

High-temperature poling enhances the piezoelectric response in relaxor-PT single crystals. Table 2 gives a comparison of the values of the longitudinal piezoelectric coefficient and the dielectric constant for poling at different temperatures. Figure 5 exhibits the maximum piezoelectric response and corresponding poling field depending on temperature. It is shown that the dielectric constant $\varepsilon^T{}_{33}/\varepsilon_0$ and piezoelectric coefficient d_{33} are increased by high-temperature poling when compared to the values for room-temperature poling. The domain size in the high-temperature poling samples is reduced as well [97,98]. The electric field strength is also lowered at elevated temperatures shown in Figure 5. It was explained that, when a DC field is applied to a single crystal at a temperature around T_C, microdomains are aligned along the applied field. When the temperature is reduced under the applied field, small ferroelectric domains with a high density of domain walls are created. The increase of d_{33} is thus attributed to the higher domain wall motion as an extrinsic contribution [76,95,97,98]. Further, at elevated temperatures, the high mobility of domain walls requires a lower electric field [76].

Table 2. Property comparison of DCP at different temperatures.

Single Crystal	Domain Configuration	DC Field (kV cm^{-1})	Poling Temp. (°C)	Domain Size (μm)	$\varepsilon_{33}/\varepsilon_0$	Loss (%)	d_{33} (pC N^{-1})
PIN–PMN–PT [a]	3T	4.0	210	0.5	13,800	0.7	1630
PIN–PMN–PT	3T	4.0	150	50.0	3000	0.4	450
0.68PMN–0.32PT [b]	3O	2.0	150	~2.0	6400	0.3	900
0.68PMN–0.32PT	3O	4.0	25	~20.0	4400	0.4	450

[a] Reference [97], [b] Reference [98].

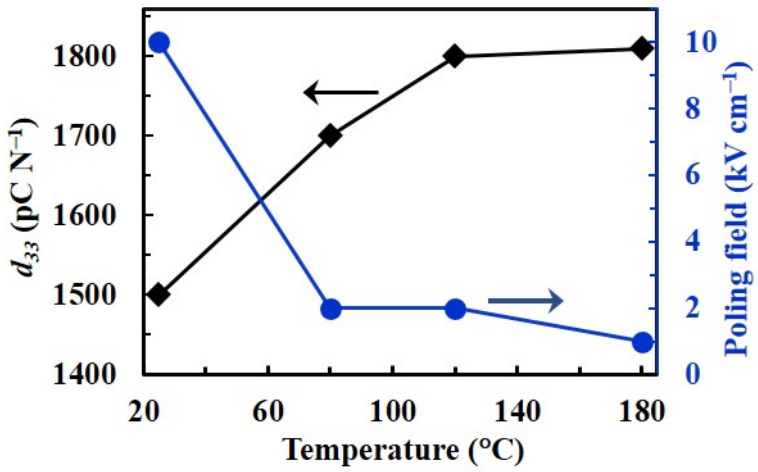

Figure 5. Temperature-dependent piezoelectric response and poling field strength in <001>-oriented PMN-30PT single crystal. Data from ref. [76].

Besides property improvement, high-temperature poling offers other benefits. Temperature stability in ferroelectric crystals is desirable for electromechanical applications. A single crystal poled at elevated temperature showed enhanced piezoelectric stability [95,98]. The d_{33} and k_{33} in <111>-poled orthorhombic PMN-PT crystal were stable up to 75 °C, which was attributed to the temperature-insensitive thickness shear coefficient d_{24} [98]. The

high-temperature poling technique also made it possible to form crack-free single domain configurations. An electric DC-field along <001> was applied to a tetragonal PIN-PMN-PT crystal at a temperature above T_C, and then on cooling, only the <001>-oriented domain was formed while the formation of non-180° domains was avoided. The reduced non-180° ferroelectric domains decreased the strain variation, resulting in achieving a crack-free single domain [94,99]. The resulting single-domain crystal showed that there was no cost to the piezoelectricity but a high mechanical quality factor [94].

High-temperature DCP is an effective technique to improve piezoelectricity. It also provides good temperature stability of the properties.

3.1.2. ACP

The ACP technique has been recently proved to be a very efficient way of improving performance in relaxor-PT crystals, including electromechanical and piezoelectric properties.

3.1.2.1. Increase of Piezoelectricity

ACP was recently proved to be efficient for engineering domains in relaxor-PT crystals. It provides greater improvement of the piezoelectric and electromechanical properties than DCP [23]. Table 3 presents a property comparison of AC- and DC-poled samples with the poling conditions. The relative dielectric permittivity and longitudinal piezoelectric coefficients of ACP in the three generations of single crystals are enhanced compared to those of DCP. It was suggested that this enhancement of the properties is attributable to ACP-induced intermediate phases and increased domain wall density, while another argument about the ACP induced enlargement of domains was proposed later. The main difference between ACP and DCP is associated with the domain structure. ACP creates well-ordered domains. In particular, it is claimed that 109° and 71° domain walls in <001>-poled rhombohedral single crystals evolve to more regular patterns with narrower widths, giving rise to a higher domain wall density [23,100–102]. The resulting high domain wall density contributes to the enhanced properties as an extrinsic contribution. Luo et al. explained the ACP effect on the formation of a uniform domain pattern. Under DCP, not all domains are oriented along the electric field, while some domains remain depolarized due to the stable DC field in the same direction [101]. Furthermore, the intrinsic contribution accounts for the improvement of piezoelectricity. ACP initiates intermediate monoclinic phases [23,101,103,104] and lattice distortion [105,106]. There is easy polarization rotation via monoclinic phases, resulting in a significant increase of the piezoelectric property [77,107,108].

In contrast to the decreased domain size and increased domain wall motion, the enlargement of domains is suggested to be a contribution to the enhanced piezoelectric response in the AC poled ferroelectric crystals. The ACP effect was explained by the repeated reversal of the electric field using a phase-field simulation, which leads to the flipping of adjacent 71° domain walls to eventually merge with each other in <001>-poled rhombohedral PMN-PT crystal. The enlargement of 71° domain widths reduces the polarization variation from the <111> polarization direction and flattens the free-energy profile. As a result, the piezoelectricity is enhanced [109]. The widened 71° domains were experimentally observed by polarized light microscopy (PLM) and high-resolution synchrotron X-ray diffraction (XRD) techniques [109,110]. The domain evolution on reduction of 71° domain wall density is consistent with other reports [102,111–113].

It was also reported that ACP-induced PNRs further support the enhancement of piezoelectricity [104,114,115]. In the single-domain tetragonal 0.25PIN-0.43PMN-0.32PT crystal, the dielectric constant after ACP is much larger than that after DCP, and the temperature-dependent dielectric constant also shows a relaxor-like frequency dispersion. This phenomenon corresponds to the existence of PNRs [104].

It should also be noted that the improvement depends on the poling conditions, including field strength, frequency, cycle, and temperature. Generally, better piezoelectric

improvement is developed at lower frequencies of the alternating current [102,111] and a higher poling temperature [116–118]. The high-temperature poling initiates multiple intermediate phases [33] and also increases the domain wall density [114]. Both intrinsic and extrinsic contributions are thus caused by high-temperature poling. At lower frequency, there is a lower energy barrier against polarization switching and lower friction or loss attributable to the property enhancement [119,120].

Table 3. Dielectric and piezoelectric property comparisons of ACP and DCP relaxor-PT single crystals under different poling conditions.

						Poling Condition			
Single Crystal (Poling)	$\varepsilon^T_{33}/\varepsilon_0$	**Differ. from DCP**	**tanδ (%)**	d_{33} **(pC N^{-1})**	**Differ. from DCP**	**Field (kV cm^{-1})**	**Freq. (Hz)**	**Cycle**	**Temp. (°C)**
0.75PMN-0.25PT (DCP) [100]	5321	/	/	1220	/	6.0–18.0	/	/	RT
0.75PMN-0.25PT(ACP)	6397	20%	/	1730	40%	12.0–18.0	20–40	20	RT
0.71PMN-0.29PT (DCP) [103]	7740	/	0.60	2030	/	5.0	/	/	50
0.71PMN-0.29PT (ACP)	8840	12%	0.98	2850	28%	12.0 ($V_{p\text{-}p}$)	20	40	50
0.70PMN-0.30PT (DCP) [103]	8490	/	0.41	2710	/	5.0	/	/	50
0.70PMN-0.30PT (ACP)	8800	4%	0.45	3050	12%	12.0 ($V_{p\text{-}p}$)	20	40	50
0.70PMN-0.30PT (DCP) [23]	6160	/	/	1650	/	10.0	/	/	RT
0.70PMN-0.30PT (ACP)	8500	38%	/	2000	21%	10.0 ($V_{p\text{-}p}$)	1.0	7	RT
0.70PMN-0.30PT (DCP) [101]	5110	/	0.39	1760	/	8.0	/	/	50
0.70PMN-0.30PT (ACP)	8330	35%	0.33	2750	56%	4.0 (rms)	0.1	20	100 to 70
0.24PIN-0.46PMN-0.30PT (DCP) [117]	5440	/	/	1810	/	4.0	/	/	50
0.24PIN-0.46PMN-0.30PT (ACP)	7000	29%	0.59	2340	29%	4.0 (rms)	10	12	90
Mn: PIN-PMN-27PT (DCP) [102]	3700	/	0.30	1350	/	5.0–15.0	/	/	RT
Mn: PIN-PMN-27PT (ACP)	5300	43%	0.30	1750	29%	20.0 ($V_{p\text{-}p}$)	0.1	20	RT

The ACP technique has been proved to be a very efficient method to increase the dielectric and piezoelectric properties of relaxor-PT single crystals.

3.1.2.2. Improvement of Transparency

The ACP technique offers another great advantage for domain engineering, in that relaxor-PT crystals could retain high multifunctional performance. Pure and modified PMN-PT systems were found to have superior properties compared with the conventional materials in optical and electro-optical applications, making them good candidates for practical needs [121,122]. AC-poled 0.72PMN–0.28PT crystal along the <001> direction was revealed with a high electro-optical coefficient (γ_{33}) of 220 pm V^{-1} and almost complete light transmittance at wavelengths higher than 400 nm. The birefringence and longitudinal piezoelectric coefficient of this sample were also improved to nearly 10 times higher and 30% greater than those of its DC-poled counterpart, respectively [109]. The improvement of the properties is associated with ACP-induced domain engineering. In Section 3.1.2.1, the mechanisms of domain change and piezoelectric enhancement are explained. The light transmittance is thus enhanced in the sample with enlarged 71° domain walls size [109,110].

3.2. Doping Strategy

Piezoelectric materials are modified for practical demands. Doping exerts two effects on Pb-based piezoelectric materials: ''hardening" and "softening". In the hardening process, acceptor-dopants facilitate defect dipoles that generate an internal field (E_i), so that they clamp the domain wall motion. Consequently, the mechanical quality factor (Q_m) increases as the dielectric and mechanical losses are reduced. In contrast, in the softening effect, donor-dopants increase the domain wall mobility. The donor-dopants leads to opposite effects to those of acceptor-dopants, including high dielectric and piezoelectric constants, a large electromechanical coupling factor, and high dielectric loss, but low Q_m and E_C [19,123]. The following section will discuss the donor and acceptor dopants in relaxor-PT single crystals and their effects on properties.

3.2.1. Hard Piezoelectric Single Crystals

The "hard" PZT ceramics are the-state-of-the-art materials for high power transducer and resonance actuator technologies. Ultrahigh piezoelectric and electromechanical properties in relaxor-PT single crystals provide piezoelectric transducers with broader bandwidths and better sensitivity compared to conventional piezoceramics [1,124]. However, the low coercive field, high mechanical loss, and low rhombohedral to tetragonal transition temperature ($T_{r\text{-}t}$) and T_C of the first generation relaxor-PT single crystals restrict their use in transducer applications [2]. Their low mechanical quality factor causes mechanical heat dissipation during transducer operations, which leads to device failure [5,125,126]. Furthermore, the coercive field of the first generation is low, so an external dc drive is used to prevent depoling, leading to extra cost [2]. It is therefore necessary for materials to have a high mechanical quality factor, a great electromechanical coupling factor, low losses, and a high coercive field in high-power and actuator applications. On the other hand, high values of Q_m, the electromechanical coupling factor k, and the piezoelectric charge constant d are the material's figure of merit ($k^2 \cdot Q_m$ or $d \cdot Q_m$) for applications [2].

The acceptor-doped ternary PIN-PMN-PT material is a promising candidate for high power applications. To meet the requirement of a high $k^2 \cdot Q_m$ or $d \cdot Q_m$, the relaxor-PT single crystals are modified by Mn dopant [18,127–129], in an analogous way to "hard" PZT ceramics. The $Mn^{3+,2+}$ cation substitutes for the Ti^{4+} cation, since the ionic sizes of both are close. Oxygen vacancy defects consequently occur in order to compensate for the charge imbalance, and it creates defect dipoles. Those defect dipoles realign in the energetically preferred direction along with the spontaneous polarization, leading to an internal field that pins domain wall motion and restricts polarization rotation. As a result, the "hardening" effect in a single crystal (the third generation relaxor-PT single crystal) is achieved [130–132]. Table 4 shows the properties of different Mn-doped Pb-based single crystals compared to those of their undoped counterparts. Among them, the Mn-doped ternary PIN-PMN-PT has drawn intensive attention. Its mechanical quality factor is 4–5 times higher than its undoped counterpart, owing to the "hardening effect" by its acceptor-dopant [18,34]. Its piezoelectric and dielectric properties values are comparable to those of its undoped counterpart. Hence, with its giant Q_m and comparable d and k values, the greater figures of merit $d \cdot Q_m$ and $k^2 \cdot Q_m$ could be achieved with Mn-doped ternary PT-relaxors. Furthermore, Q_m, being on the order of >1000 in these single crystals, is comparable to those of "hard" PZTs. Higher k and d on the order of >0.90 and >1000, respectively, are also found. The figure of merit value, therefore, is far superior to that of the conventional PZT ceramics [2,17,18,124,130]. After modifying the relaxor-PT single crystal, it was also confirmed to be stable in external fields. The coercive field is 2 to 3 times higher than that of the first generation of single crystals [2,35,130,131] and slightly greater than that of its second generation counterparts with the same domain structure due to the acceptor-induced internal field [17,34,130,133]. The existence of internal bias in the third-generation crystals provides higher allowable ac drive fields and could avoid the depolarization [134] due to stabilized domain motion. In Table 4, it is also shown that single-domain crystals demonstrate a much higher quality factor compared to those of multi-domain crystals due to the fact that there is the least polarization rotation involved [36,124,131,135]. All of these property improvements are ascribed to the defect-dipole-induced internal field, which clamps domain wall motion and constrains the polar rotation.

Mn-doped ternary PIN-PMN-PT and PMN-PZT single crystals are hence suitable materials for use in high power transducer applications due to high Q_m and E_C values, low losses, and a comparable piezoelectric response and electromechanical coupling factor.

Table 4. Property comparisons of pure PMN-PT, pure and Mn-doped PIN-PMN-PT, pure and Mn-doped 0.88PZN-0.12PT, pure and Mn-doped 0.4PMN–0.25PZ–0.35PT, and Mn-doped 0.68PIN-0.32PT single crystals.

Material (Domain State)	Orientation	T_C (°C)	E_C (kV/cm)	$\varepsilon^T{}_{33}/\varepsilon_0$	tanδ (%)	Q_{33}	k_{33}	d_{33} (pC/N)	Growth Method	Ref.
0.70PMN–0.33PT	<001> [c]	155	2.8	8200	/	100	0.94	2820	MB [b]	[2]
PIN–PMN–PT (MPB) [a]	<001> [c]	197	5.5	7244	/	120	0.95	2742	MB	[2]
PIN-PMN-PT:Mn (2R) [a]	<011> [c]	197	5.1	3523	0.6	1000	0.90	1053	MB	[130]
0.27PIN-0.46PMN-0.27PT:Mn (1R)	<111> [c]	194	9.1	1299	/	1200	0.346	95	MB	[131]
0.26PIN-0.42PMN-0.32PT:Mn (1O)	<011> [c]	208	5.6	1240	0.1	1230	0.70	267	MB	[35]
0.26PIN-0.42PMN-0.32PT:Mn (4O)	<001> [c]	208	4.9	4280	0.4	300	0.91	1370	MB	[35]
0.88PZN-0.12PT:Mn	<110> [c]	180	8.6	5300	0.4	750	0.60	500–600	CFG [c]	[128]
0.88PZN-0.12PT	<110> [c]	185	12.3	5500	/	150	0.615	530	CFG	[128]
0.4PMN–0.25PZ–0.35PT:Mn	<001> [c]	203	6.3	3410	0.2	1050	0.92	1140	SSCG [d]	[17]
0.4PMN–0.25PZ–0.35PT	<001> [c]	211	4.5	4850	0.5	100	0.93	1530	SSCG	[17]
0.68PIN-0.32PT:Mn	<001> [c]	231	9.7	1284	1.0	/	0.80	730	CFG	[129]

[a] The exact composition of the single crystals are not given. [b] The Modified Bridgman method. [c] Conventional flux growth method. [d] Solid state conversion growth method.

3.2.2. Soft Piezoelectric Single Crystals

For ultrasound transducer technologies, the high sensitivity of a device requires materials with a large electromechanical coupling factor, great piezoelectric coefficient, and high elastic compliance [2,136]. In order to improve the electromechanical factor and piezoelectric response, donor additives are introduced into conventional PZT ceramics. The resulting phenomenon is a "softening" effect opposite to that of "hardening". In donor-doped piezoelectric perovskite materials, an A-site vacancy is induced to neutralize charge imbalance. A pair of La^{3+} cations, for instance, create one Pb^{2+}-vacancy. The Pb-vacancy enhances the domain wall mobility, leading to a low coercive field, large dielectric constant and piezoelectric coefficient, a high electromechanical coupling factor, and high elastic compliance, but a reduced mechanical quality factor [19]. The donor-dopant La^{3+} in PZT has been intensively studied because it increases the dielectric constant due to relaxor behavior and is suitable for electro-optical applications [137–141]. Sm^{3+} has recently drawn attention due to its contribution to a giant electromechanical coupling factor and drastic increase of the piezoelectric coefficient in relaxor-PT systems [142–150]. A certain addition of Sm dopant is confirmed to lead to the highest values of d_{33}, being on the order of 1500 pC N^{-1}, and $\varepsilon^T_{33}/\varepsilon_0$ being on the order of 13,000 in PMN-PT ceramic, and d_{33} being on the order of 4100 pC N^{-1} and $\varepsilon^T_{33}/\varepsilon_0$ of ~12,000 in PMN-PT single crystal, respectively [24,146]. Alongside the "softening" effect, A-site substituted Sm^{3+} doping enhances the local heterogeneity that minimizes the local free energy via competition between the bulk and interfacial energies. The lower free energy facilitates a large dielectric constant and a large piezoelectric coefficient [146,151]. It is also important to note that the ionic size of samarium doping is the most suitable formation among other rare-earths ions to enhance the local heterogeneity, so this dopant results in the largest property values [24,152]. Donor dopants induce increased dielectric constant but a decreased Curie temperature [24,143,146]. It was explained that the random fields induced by donor dopants affect the Curie temperature [24,153].

Donor-doped relaxor ferroelectric materials demonstrate outstanding dielectric and piezoelectric performances, owing to the local structural heterogeneity in addition to "softening" effect, where the local structural heterogeneity plays the dominant role. The improved properties are suitable to use for enhancing actuator and medical imaging devices.

4. Anisotropic Features

The relaxor-PT single crystals exhibit highly anisotropic behavior, which greatly benefits the superior piezoelectricity. Understanding the anisotropy of relaxor-PT single crystal is important for device design. When relaxor-PT is poled along one of crystallographic

directions, different domain configurations or single domains will be formed. For instance, when the orthorhombic phase is poled along the <111>, <011> and <001> directions, this will form 3O, 1O, and 4O domain configurations, respectively. When the rhombohedral phase is poled along <111>, <011> and <001> directions, this will achieve 1R, 2R, and 4R configurations, respectively. For tetragonal phase, 3T, 2T and 1T domain configurations are respectively achieved when poled along the <111>, <011> and <001> directions [1,75,77]. Such formation of domain structures is the so-called "domain engineering" [75], and this phenomenon leads to highly anisotropic piezoelectric tensors in relaxor-PT single crystals. The degree of piezoelectric anisotropy is defined by the "anisotropic factor" as following ratio [154]:

$$\left(\frac{d_{15}}{d_{33}}\right) = 2\frac{Q_{13}}{Q_{33}}\left(\frac{\chi_{11}}{\chi_{33}}\right) \quad (1)$$

where, d_{33} and d_{15} are the longitudinal and shear piezoelectric coefficients, Q_{33} and Q_{13} are the longitudinal and shear electrostrictive coefficients, and χ_{33} and χ_{11} are the longitudinal and transverse dielectric susceptibilities, respectively.

Table 5 summarizes the anisotropy of the principal properties in the second generation relaxor-PT crystals. Figure 6 compared the anisotropic factors of different ferroelectric single crystals. Based on the piezoelectric values from Table 5 and Figure 6, the anisotropic factors are high in relaxor-PT single crystals, indicating that relaxor-PT crystals are highly anisotropic.

It was shown that the shear piezoelectric coefficient is the highest in the single domain configuration [37,133,153–158]. From calculations of the orientation dependence, the maximum dielectric constant was observed in the direction perpendicular to the poling electric field, i.e., transverse dielectric constant, near the ferroelectric-to-ferroelectric phase transition in single domain state [156,159]. The high value of the shear piezoelectric coefficient is related to the change in the transverse dielectric constant that arises from polarization rotation. Owing to free-energy profile flattening, polarization rotation simply occurs in the vicinity of a ferroelectric-to-ferroelectric phase transition [160]. For relaxor-PT single crystals, there is a high possibility of different phase transitions induced by composition, electric field, or temperature that lead to easy rotation of the polar vector [77,154]. The longitudinal piezoelectric coefficient has a low value, however, in the single domain configuration. This response is attributed to the polarization extension. The polarization extends towards an electric field direction when is the electric field applied along the polar direction. Therefore, the longitudinal piezoelectric property is ascribed to change in the longitudinal dielectric constant [154,160].

Table 5. Anisotropic properties of the second generation relaxor-PT ferroelectric crystals.

Composition	Domain Configur.	$\varepsilon_{33}^T/\varepsilon_0$	$\varepsilon_{11}^T/\varepsilon_0$	$\varepsilon_{22}^T/\varepsilon_0$	d_{15} (pC·N^{-1})	d_{31} (pC·N^{-1})	d_{32} (pC·N^{-1})	d_{33} (pC·N^{-1})	k_{31}	k_{33}	k_{15}	Ref.
PIN–PMN–28PT	2R	2920	5000	1030	2203	460	−1156	782	0.67	0.87	0.91	[133]
PIN–PMN–28PT	1R	702	6286	/	2190	−34	/	74	0.13	0.36	0.92	[159]
PIN–PMN–33PT	4O	7244	10,081	/	232	−1337	/	2742	0.65	0.95	0.20	[15]
PIN–PMN–33PT	1O	1500	8070	30,000	4550	153	−346	350	0.44	0.74	0.96	[157]
PIN–PMN–(39–41)PT	1T	1090	15,000	/	2350	−200	/	530	0.50	0.84	0.85	[37]

A high longitudinal piezoelectric coefficient exists in multi-domain configurations. From the calculation of the orientation dependence, maximum values of d_{33} are found at a certain angle away from the spontaneous polarization direction, indicating a contribution from the polarization rotation [37–39,156,161–163]. The longitudinal piezoelectric response in multi-domain single crystal also benefits from the shear piezoelectric phenomenon. The greatest values of d_{33} were revealed in 4O and 4R domain-engineered single crystals [5,15,38–40,163–167]. Furthermore, another anisotropic source contributes to the high piezoelectric response. As seen in expression (1), the anisotropy of piezoelectricity is also dependent on the anisotropy of electrostrictive coefficients. From calculations of the orientation dependence, the maximum electrostrictive coefficient was found in the

<100> direction where similar values are observed among the *R*, *O*, and *T* phases shown in Figure 7a. The minimum value was calculated in the <111> direction, and similar values were also observed in the three phases. Thus, the electrostrictive coefficient is not sensitive to ferroelectric phase. The change of the electrostrictive coefficient is more related to the oxygen octahedral in Figure 7b. For <001> direction phases, one oxygen ion moves upwards in order to release the B-O pair potential in Figure 7b (left). For the <111> direction, three oxygen ions along a perpendicular direction to the <111> direction need to be displaced, and this motion reduces the electrostrictive property Figure 7b (right). Therefore, under an electric field along the <001> direction, the maximum value of the electrostrictive coefficient contributes to the ultrahigh value of d_{33} in 4R and 4O domain-engineered single crystals [40,168].

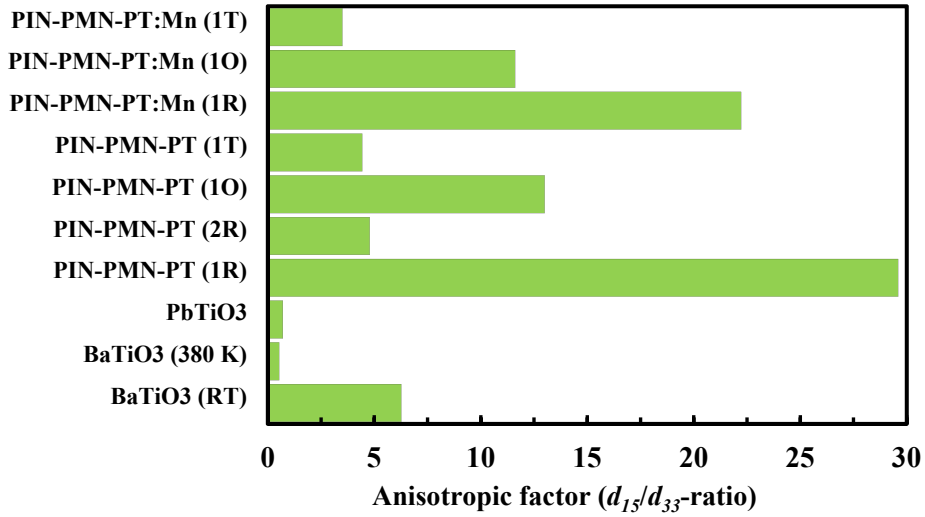

Figure 6. Anisotropic factors of various ferroelectric single crystals. Data from references [35–37,131,154,157,159,166,167].

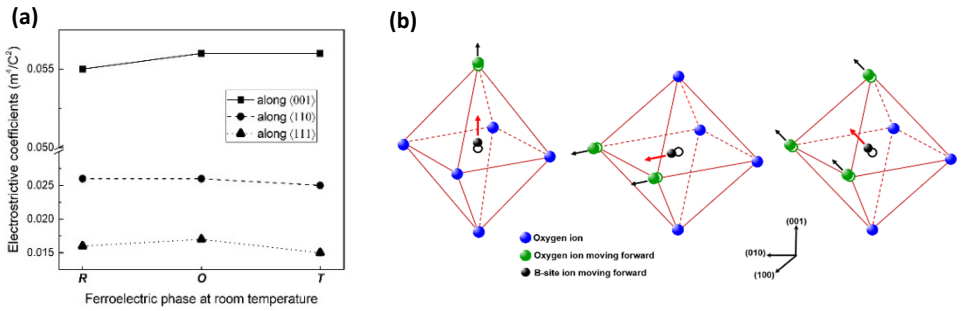

Figure 7. (**a**) Calculated longitudinal electrostrictive coefficients along ⟨111⟩, ⟨110⟩, and ⟨100⟩ directions for rhombohedral, orthorhombic and tetragonal phases [40]. (**b**) Oxygen ion displacement in octahedral structure with three different polarization directions: <001> (left), <110> (middle) and <111> (right).

Intense attention was focused on the '2R' domain configuration of <011>-poled rhombohedral single crystal. The uniqueness of this configuration is due to the simultaneously high values of its longitudinal, shear, and transverse piezoelectric properties. Furthermore, it presents a greater mechanical quality factor than that of the 4R domain configuration because of the lower polarization rotation angle [42,169–172].

Another important anisotropic property of relaxor-PT crystals was found in the mechanical quality factor in modified relaxor-PT ferroelectric crystals [173–176]. Generally, in relaxor-PT single crystal, Q_{33} is high but Q_{15} is lower. This is due to the fact that a larger polarization rotation angle is involved in the case of the shear property than that

of longitudinal response. Improvement of the mechanical quality factor in Mn-modified single crystal is because the defect dipole-induced internal bias inhibits polarization rotation [18,34,35,177]. There is another pinning effect that is revealed when an electric field is applied along the lateral direction. Zheng et al. determined that in <001>-poled PIN-PMN-27PT:Mn single crystal, the internal bias was 1.44 kV/cm with the external electric field parallel to the poling direction, while it was 0.12 kV/cm with a perpendicular external field. In addition, with a perpendicular electric field, the external contribution to piezoelectricity is 3.7 times lower than that of the parallel electric field. With manganese doping, however, Q_{33} and Q_{15} are improved to 360% and 400%, respectively, indicating that another pinning mechanism serves for the shear direction [178]. In unpoled ferroelectrics, neutral domain walls minimize elastic energy. In a manganese-doped sample, however, 109° charged domain walls are favourable. In charged domain walls, due to the repelling force of opposite charges, Mn ions stay in head-to-head positions in the domain wall while oxygen vacancies are pushed to the tail-to-tail position. Consequently, a strong electrostatic force is created that is hard to break by a transverse electric field. Such charged domains clamp domain wall motion and inhibit polarization rotation in the lateral direction rather than the internal field [178,179].

5. Application Perspectives

In general, the giant electromechanical coupling factor and ultrahigh piezoelectric property in relaxor-PT single crystals enable them to carry out the higher broadband operation and exhibit better sensitivity in transducer applications when compared to those properties in traditional PZT ceramics [2]. This section discusses perspectives on the current progress on relaxor-PT crystals and provides some current examples for electromechanical applications.

5.1. Doping Advantage

Piezoelectric materials are widely applied in underwater acoustic transducers. For underwater acoustics, the most common designs comprise the cymbal, 1–3 composite, and Tonpilz designs [125,180]. PMN-PT single crystals have been used as the active element in Tonpilz transducers, and they featured an expanded bandwidth and reduced stack length, owing to the high electromechanical coupling factor of the single crystals [181–183]. Despite some performance improvements in the Tonpilz design, a crucial issue has been the self-heating in piezoelectric elements, which is associated with a low mechanical quality factor and high loss of the single crystals. A Mn-modified PIN-PMN-PT element in the Tonpilz design was proven to exhibit excellent energy conversion with the least heat dissipation when compared to its PMN-PT and PIN-PMN-PT counterparts [177,180]. In addition, the Mn-modified Tonpilz design showed great stability of principal properties over operational limits of driving field and temperature. In Figure 8, the bandwidths of Tonpilz are compared with three generation of the single crystals and the conventional ceramic material. A Mn-modified transducer also exhibited superior bandwidth and energy source level to those of conventional ceramic-made transducers and higher mechanical quality factor compared to PMN-PT and PIN-PMN-PT transducers [184]. All these improvements are attributed to restricted polarization rotation and pinned domain wall motion caused by the "hardening effect". Low heat generation was also observed in other types of underwater acoustic devices when using Mn-doped single crystal. For instance, a Mn: PIN-PNM-PT flextensional transducer exhibits lower heat generation than unmodified single crystals and PZT polycrystals [185].

Relaxor-PT single crystals were confirmed to be suitable for use in a number of medical applications, including ultrasound diagnostic imaging, ultrasound therapy, and high intensity focused ultrasound, to mention a few [136,186]. The type of medical transducer and its application frequency range depends on the biological tissues [136]. The most important demand for medical transducers is for the improvement of imaging. Although the imaging depends on various characteristics of the device, the electromechanical coupling of the

piezoelectric element makes the main contribution to the image resolution. Therefore, enhancement of the coupling factor is a crucial necessity for medical application [136,186]. Furthermore, high power and high temperature medical transducers is another important issue for medical devices. In particular, medical therapy devices work on the resonance frequency, signifying the requirement of a piezoelectric element with a high mechanical quality factor and low loss [187]. The figure of the merit in medical applications, hence, is derived from high k. Overall, the relaxor-PT single crystals enhance the bandwidth and sensitivity of medical transducers [2,13,187–190].

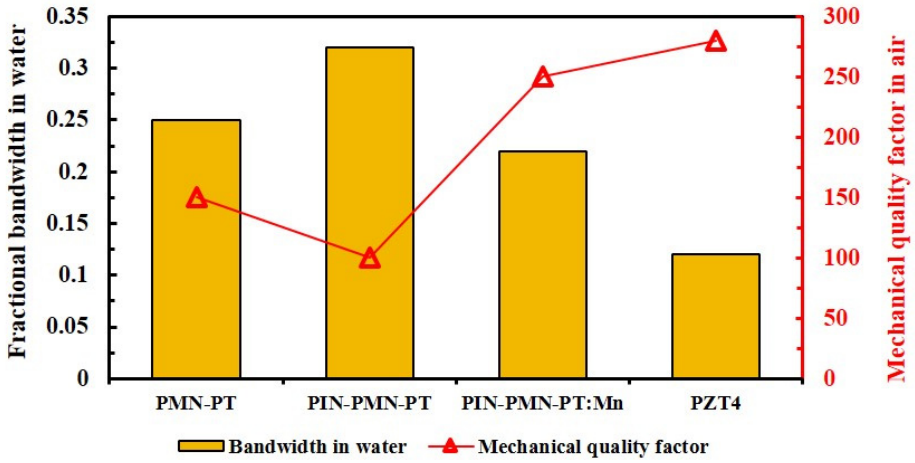

Figure 8. Bandwidths and quality factors of Tonpilz-design transducers made of PMN-PT, PIN-PMN-PT, Mn-modified PIN-PMN-PT crystals and PZT4 ceramic [184].

Medical transducers operate at higher frequencies than their underwater acoustic counterparts [2,136]. Principally, a higher frequency transducer requires smaller sizes of its piezoelectric material [2,186]. However, scaling degrades material's property. Figure 9 shows piezoelectric coefficient of PMN-PT single crystal which is a function of thickness. Geometric features on relaxor-PT single crystals were shown to enhance the performance of miniaturized transducers [191,192]. For intravascular ultrasound transducer imaging, dimpled PMN-PT crystals at 30–80 MHz demonstrated a broader bandwidth, higher centre frequency, and sharper focus of images than those of their plane element counterparts, and the enhancement is associated with thickness reduction and multi-resonances varying along the concave surface, but at the cost of a slight increase of the insertion loss [193,194]. The piezoelectric/epoxy composite design is one of the most promising approaches to improve transducer performance [187,190,195,196]. Relaxor-PT single crystals were successfully applied in the composite transducers [197–199]. The 1–3 crystal/polymer composite transducer is of particular interest. In this design, the best aspect ratio of the active element offers a great coupling factor, the low acoustic impedance provides better matching of energy between the transducer and the medium, and the composite array reduces lateral vibration modes [187,198–201]. Therefore, the 1–3 composite design improves transducer performance much more than the single piezo-element design does.

To meet the requirements of a good figure of merit (FOM) for $k^2 \cdot Q_m$, Mn-doped single crystal was applied in electromechanical medical devices. For instance, a Mn-modified PIN-PMN-PT-based needle transducer showed high performance up to 140 °C. Mn doping lowers the heat dissipation and allows the transducer to operate at elevated temperatures [202].

Drastic increases in dielectric and piezoelectric properties in donor-doped "soft" single crystals are very advantageous for electromechanical applications. Rare-earth Sm-doped PMN-PT single crystal possesses the largest values of d_{33} and $\varepsilon_{33}/\varepsilon_0$ among all the piezoelectric materials. These properties could be of particular benefit to high frequency

medical transducers where giant property values would be less affected by the scaling process [24,146].

5.2. Poling Advantage

High frequency electromechanical devices require small-sized piezoelectric materials as active elements. The scaling effect restricts the improvement of the electromechanical properties of ferroelectric single crystals for high frequency transducers. It was reported that smaller ferroelectric domains in 1–3 PIN-PMN-PT/epoxy transducer resulted in better electromechanical improvement than in a larger domain PMN-PT crystal, where the surface boundary clamped large domains [203,204]. It was also reported that high-temperature DC poling induced small-sized ferroelectric domains in relaxor-PT single crystal [76,95,98]. Therefore, small domains of single crystals induced by high-temperature poling could alleviate the scaling effect and achieve better electromechanical improvement in high-frequency transducers.

ACP-induced improvements of piezoelectric and electromechanical properties in relaxor-PT single crystals have made it possible to further broaden the bandwidth and thus, increase the sensitivity at a greater distance in transducer devices [205,206].

The piezoelectric and dielectric performances in Mn-doped PIN-PMN-PT are lower than the first- and the second-generation crystals [2,18]. The AC-poling technique could help reduce this gap. In AC-poled Mn-doped PIN-PMN-PT, ${\varepsilon^T}_{33}/\varepsilon_0$ and d_{33} increased to 45% and 29%, respectively (as shown in Table 2). Longitudinal and lateral electromechanical coupling factors were also improved by ACP [100,114]. Therefore, the resulting property changes resulted in significant enhancement of the FOM $k^2 \cdot Q_m$ in transducer applications.

AC-poled relaxor-PT single crystals were also studied to understand the scaling effect. Increases of dielectric and piezoelectric properties in AC-poled PMN-PT crystals were higher than those in its DC-poled counterpart when the sample's thickness was as low as 100 μm. A scaling effect was observed in a 100 μm thick sample, but it was weak when the thickness was larger than 200 μm [207]. The weak scaling effect in AC-poled samples could support improvements of high-frequency transducer technology.

High multifunctional performance in ferroelectric materials has always been a challenge. For optical and electro-optical devices, searching for a material that has good properties in terms of both optics and piezoelectricity is a difficult quest. $LiNbO_3$ is a prototype material for optical communication and shows good transparency, but its piezoelectricity and electromechanical coupling are too low [116]. Another transparent material, La-doped PZT ceramic possesses good piezoelectricity and a good electro-optical coefficient, but it shows a polarization-dependent scattering loss [115,208]. The high multifunctional performance of AC-poled PMN-PT crystal was discussed in Section 3.1.2. Therefore, AC-poled relaxor single crystal is shown to be able to compensate for the disadvantages of the conventional materials and opens new frontiers for the improvement of optical and electro-optical devices [109].

5.3. Anisotropic Advantage

From the applications point of view, the majority of studies on relaxor-PT crystals have been focused on the rhombohedral composition on the left side of the MPB or the pure MPB composition, owing to their ultrahigh piezoelectric and electromechanical properties. Nevertheless, the tetragonal single crystals have some advantages over their rhombohedral counterparts, having higher coercive fields, greater T_C, and no occurrence of a ferroelectric-to-ferroelectric phase transition up to T_C [154,209–211]. The anisotropic features of tetragonal relaxor-PT single crystals offer further potential for transducer applications. For high-frequency transducer devices, the piezoelectric element needs to be scaled down to a thin layer [136]. As mentioned above, however, owing to the inferior mechanical strength at high frequencies of relaxor-PT crystals, the scaling involves property deterioration. Piezoelectric response reduces as the thickness of sample decreases shown in Figure 9. The <111>-oriented tetragonal PIN-PMN-PT single crystal offers a higher fre-

quency constant than those of its rhombohedral counterpart and of PZT ceramics, which is associated with a high elastic stiffness constant along the <111> direction in the perovskite structure. In addition, this single crystal shows a very high free and clamped longitudinal dielectric constant that benefits from the transverse dielectric constant of its single domain structure [212]. Hence, such advances in <111>-oriented tetragonal PIN-PMN-PT make it a favourable candidate for high-frequency transducer application. The '1T' single domain tetragonal Mn: PIN-PMN-PT crystal possesses a large Q_m > ~2000. The high value of Q_m is related to the reduction of polarization rotation and the absence of domain wall motion, due to the single domain state and doping-induced E_i. Consequently, such a Mn-modified tetragonal single crystal provides the highest FOM $d \cdot Q$, giving it a perfect potential for high power transducer applications [36].

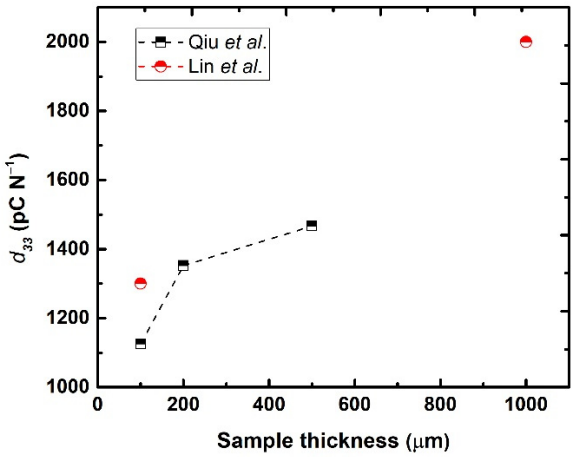

Figure 9. Longitudinal piezoelectric coefficient of PMN-PT single crystal is a function of sample's thickness [207,211].

The anisotropic characteristic of relaxor-PT single crystal also offers better performance in the design of actuators [213,214]. The Zt ± 45° cut of <011>-oriented rhombohedral relaxor-PT crystal exhibits excellent face-shear properties of d_{36} and k_{36}, as well as high stability over different ranges of temperature and driving field [171,172]. The advantages of face-shear mode in <011>-poled Zt ± 45° cut PIN-PMN-0.30PT crystal allow to be used to develop an ultrasound motor with doubled values of its power density of 1.48×10^{-4} W/mm^3 and its electromechanical coupling factor of 0.65, as well as a lower driving frequency (72 kHz), when compared to the prototype k_{31} mode PZT motor. Furthermore, the unique in-plane anisotropy of <011>-poled Zt ± 45° cut PMN-0.28PT single crystal was proven to be feasible material for linear ultrasound actuators [215]. The asymmetric and non-isomorphic face-shear mode of this sample provides the ultrasound motor with a greater driving field of 1.5 N under a lower driving voltage of 22 V_{pp} [216].

The low driven voltage and high driving field of face-shear mode have been paid immense attention. Heat dissipation is a serious concern, however, when ultrasound actuators operate at their resonance frequency. Hence, without improvement of the mechanical quality factor, it is impossible to achieve further advances in actuator applications using relaxor-PT single crystals. A k_{31}-mode typical ultrasound motor was developed using Mn-modified PIN-PMN-PT single crystal poled along the <001> direction. The motor achieved better output performance compared to those based on both PZT ceramic and face-shear relaxor-PT single crystal. The output power of Mn-modified motor is compared to those of face-shear and ceramic motors in Figure 10. The output power density of 0.45 W/cm^3 was three times larger than those of a PZT ceramic motor and a face-shear relaxor-PT crystal motor. The reason for the enhancement was the low thermal generation, and in particular, it is ascribed to the "hardening effect" induced by dipole-defects arising from Mn-modification [217].

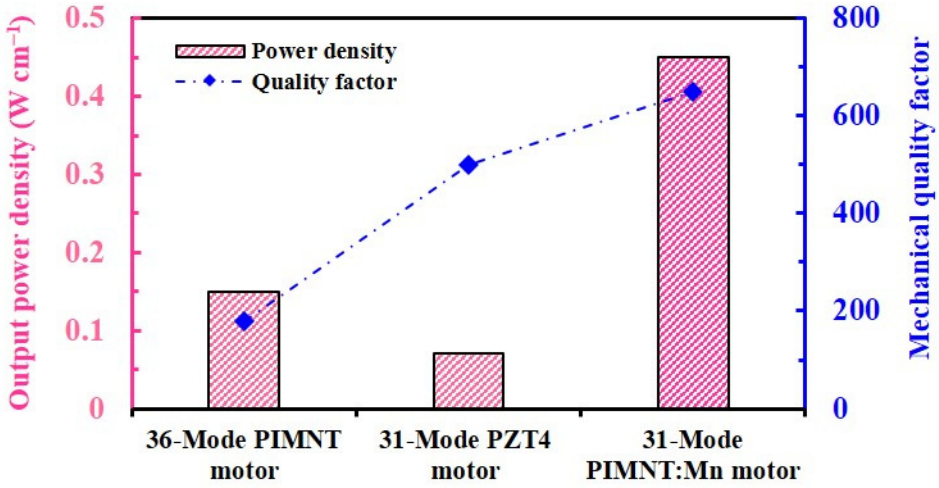

Figure 10. Output powers of 36-mode single crystal, 31-mode Mn-modified. single crystals and 31-mode PZT4 ceramic ultrasound motors [174,214,217].

6. Summary

The current progress on relaxor-PT ferroelectric crystals and their opportunities in electromechanical applications have been reviewed. Two single crystal growth methods were emphasized, the modified Bridgman and solid-state conversion growth methods. These methods provide an adequate way of fabricating large quantities of relaxor-PT single crystals. Both methods have struggled with the quality of their as-grown crystals, although recent progress on these methods has been solving this issue.

Doping was proven to be an efficient strategy for achieving improvements in piezoelectric and electromechanical performance. Acceptor doping exhibits a "hardening" effect, which leads to improved mechanical coupling and reduced loss, while donor doping demonstrates a "softening" effect that results in enhanced piezoelectricity and electromechanical coupling. In the "hard" piezoelectric single crystals, doping-induced defect-dipoles pin domain wall motion and restrict polarization rotation, so that heat dissipation is reduced. Therefore, "hard" single crystals benefit the high-power transducer and ultrasonic motor applications. Enhanced dielectric and piezoelectric properties induced by donor dopants are advantageous, especially for high-frequency transducer devices. The poling technique is another effective way of increasing piezoelectric and electromechanical properties. High-temperature DC-poling was confirmed to increase the piezoelectric response. Recently, AC-poling has been intensively studied. This technique offers much more improvement of dielectric and piezoelectric properties than for the DC-poling method in relaxor-PT crystals. This technique also increases coupling factors. The induced property improvements in the single crystals pave the way for the improvement of diverse electromechanical applications. The anisotropy of relaxor-PT single crystals always offers unique features in the material's behavior.

7. Prospectives

Intensive attempts have been focused on improving the compositional homogeneity of the as-grown crystals using the modified Bridgman growth method. SSCG is an alternative method to produce more homogeneous crystals at low cost. Meanwhile, since melting does not occur during SSCG, relaxor-PT crystals with refractory components have been successfully achieved. It is expected relaxor-PT crystals with different end member components can increase the Curie temperature and coercive field, enabling a broader usage temperature range and drive stability compared with their binary PMN-PT and ternary PIN-PMN-PT counterparts.

Ferroelectric materials must be poled to exhibit piezoelectricity. The poling condition is extremely important for a ferroelectric material, which has been actively studied in the

last many decades. ACP technique attracts immense attention in relaxor-PT ferroelectric crystals because it greatly benefits the piezoelectric and dielectric properties. However, the underlying mechanism responsible for the ACP-induced property enhancement is still open. Meanwhile, the reliability and stability of the property under different external stimuli, including electric field, stress field and temperature, are not yet fully understood. Thus further research on the ACP poled ferroelectric crystals is desired in order to take full advantage of the enhanced properties for practical electromechanical applications.

Author Contributions: Conceptualization, L.B.; writing—original draft preparation, L.B.; writing—review and editing, Z.C.; supervision, Z.C. All authors have read and agreed to the published version of the manuscript.

Funding: This research was funded by ONRG (grant number N62909-18-12168) and ONRG (grant number N62909-21-1-2037).

Institutional Review Board Statement: Not applicable.

Informed Consent Statement: Not applicable.

Data Availability Statement: Not applicable.

Acknowledgments: The authors want to thank Shujun Zhang for his valuable comments and suggestions on this review paper and strong support for LB's research. The authors also thank Tania Silver for the detailed language editing.

Conflicts of Interest: The authors declare no conflict of interest.

References

1. Zhang, S.; Li, F. High performance ferroelectric relaxor-$PbTiO_3$ single crystals: Status and perspective. *J. Appl. Phys.* **2012**, *111*, 031301. [CrossRef]
2. Zhang, S.; Li, F.; Jiang, X.; Kim, J.; Luo, J.; Geng, X. Advantages and challenges of relaxor-$PbTiO_3$ ferroelectric crystals for electroacoustic transducers—A review. *Prog. Mater. Sci.* **2015**, *68*, 1–66. [CrossRef] [PubMed]
3. Zhang, S.; Li, F.; Yu, F.; Jiang, X.; Lee, H.Y.; Luo, J.; Shrout, T.R. Recent developments in piezoelectric crystals. *J. Korean Ceram. Soc.* **2018**, *55*, 419–439. [CrossRef]
4. Trolier-McKinstry, S.; Zhang, S.; Bell, A.J.; Tan, X. High-performance piezoelectric crystals, ceramics, and films. *Annu. Rev. Mater. Res.* **2018**, *48*, 191–217. [CrossRef]
5. Park, S.E.; Shrout, T.R. Relaxor based ferroelectric single crystals for electro-mechanical actuators. *Mater. Res. Innov.* **1997**, *1*, 20–25. [CrossRef]
6. Luo, H.; Xu, G.; Wang, P.; Yin, Z. Growth and characterization of relaxor ferroelectric PMNT single crystals. *Ferroelectrics* **1999**, *231*, 97–102. [CrossRef]
7. Shimanuki, S.; Saito, S.; Yamashita, Y. Single crystal of the $Pb(Zn_{1/3}Nb_{2/3})O_3$–$PbTiO_3$ system grown by the vertical Bridgeman method and its characterization. *Jpn. J. Appl. Phys.* **1998**, *37*, 3382. [CrossRef]
8. Zhang, S.; Lebrun, L.; Jeong, D.Y.; Randall, C.A.; Zhang, Q.; Shrout, T.R. Growth and characterization of Fe-doped $Pb(Zn_{1/3}Nb_{2/3})O_3-PbTiO_3$ single crystals. *J. Appl. Phys.* **2003**, *93*, 9257–9262. [CrossRef]
9. Zhang, S.; Randall, C.A.; Shrout, T.R. Characterization of perovskite piezoelectric single crystals of $0.43BiScO_3$–$0.57PbTiO_3$ with high Curie temperature. *J. Appl. Phys.* **2004**, *95*, 4291–4295. [CrossRef]
10. Zhang, S.; Rhee, S.; Randall, C.A.; Shrout, T.R. Dielectric and piezoelectric properties of high Curie temperature single crystals in the $Pb(Yb_{1/2}Nb_{1/2})O_3$–$xPbTiO_3$ solid solution series. *Jpn. J. Appl. Phys.* **2002**, *41*, 722. [CrossRef]
11. Zhang, S.; Lee, S.M.; Kim, D.H.; Lee, H.; Shrout, T.R. Characterization of high T_C $Pb(Mg_{1/3}Nb_{2/3})O_3$-$PbZrO_3$-$PbTiO_3$ single crystals fabricated by solid state crystal growth. *Appl. Phys. Lett.* **2007**, *90*, 232911. [CrossRef]
12. Tian, J.; Han, P.; Huang, X.; Pan, H.; Carroll, J.F., III; Payne, D.A. Improved stability for piezoelectric crystals grown in the lead indium niobate–lead magnesium niobate–lead titanate system. *Appl. Phys. Lett.* **2007**, *91*, 222903. [CrossRef]
13. Hosono, Y.; Yamashita, Y. Piezoelectric ceramics and single crystals for ultrasonic medical transducers. *J. Electroceram.* **2006**, *17*, 577–583. [CrossRef]
14. Zhang, S.; Luo, J.; Hackenberger, W.; Shrout, T.R. Characterization of $Pb(In_{1/2}Nb_{1/2})O_3$–$Pb(Mg_{1/3}Nb_{2/3})O_3$–$PbTiO_3$ ferroelectric crystal with enhanced phase transition temperatures. *J. Appl. Phys.* **2008**, *104*, 064106. [CrossRef]
15. Liu, X.; Zhang, S.; Luo, J.; Shrout, T.R.; Cao, W. Complete set of material constants of $Pb(In_{1/2}Nb_{1/2})O_3$–$Pb(Mg_{1/3}Nb_{2/3})O_3$–$PbTiO_3$ single crystal with morphotropic phase boundary composition. *J. Appl. Phys.* **2009**, *106*, 074112. [CrossRef]
16. Zhang, S.; Li, F.; Sherlock, N.P.; Luo, J.; Lee, H.J.; Xia, R.; Meyer, R.J., Jr.; Hackenberger, W.; Shrout, T.R. Recent developments on high Curie temperature PIN–PMN–PT ferroelectric crystals. *J. Cryst. Growth* **2011**, *318*, 846–850. [CrossRef] [PubMed]

17. Zhang, S.; Lee, S.M.; Kim, D.H.; Lee, H.Y.; Shrout, T.R. Characterization of Mn-modified $Pb(Mg_{1/3}Nb_{2/3})O_3$-$PbZrO_3$-$PbTiO_3$ single crystals for high power broad bandwidth transducers. *Appl. Phys. Lett.* **2008**, *93*, 122908. [CrossRef] [PubMed]
18. Luo, J.; Hackenberger, W.; Zhang, S.; Shrout, T.R. A high Qm relaxor ferroelectric single crystal: Growth and characterization. In Proceedings of the 2010 IEEE International Ultrasonics Symposium, San Diego, CA, USA, 11–14 October 2010; pp. 68–71.
19. Jaffe, B.; Cook, W.R.; Jaffe, H. *Piezoelectric Ceramics*; Academic Press: New York, NY, USA, 1971.
20. Zhao, X.; Fang, B.; Cao, H.; Guo, Y.; Luo, H. Dielectric and piezoelectric performance of PMN–PT single crystals with compositions around the MPB: Influence of composition, poling field and crystal orientation. *Mater. Sci. Eng. B* **2002**, *96*, 254–262. [CrossRef]
21. Colla, E.; Yushin, N.K.; Viehland, D. Dielectric properties of $(PMN)_{(1-x)}(PT)_x$ single crystals for various electrical and thermal histories. *J. Appl. Phys.* **1998**, *83*, 3298–3304. [CrossRef]
22. Guo, Y.; Luo, H.; Chen, K.; Xu, H.; Zhang, X.; Yin, Z. Effect of composition and poling field on the properties and ferroelectric phase-stability of $Pb(Mg_{1/3}Nb_{2/3})O_3$–$PbTiO_3$ crystals. *J. Appl. Phys.* **2002**, *92*, 6134–6138. [CrossRef]
23. Chang, W.Y.; Chung, C.C.; Luo, C.; Kim, T.; Yamashita, Y.; Jones, J.L.; Jiang, X. Dielectric and piezoelectric properties of $0.7Pb(Mg_{1/3}Nb_{2/3})O_3$-$0.3PbTiO_3$ single crystal poled using alternating current. *Mater. Res. Lett.* **2018**, *6*, 537–544. [CrossRef]
24. Li, F.; Cabral, M.J.; Xu, B.; Cheng, Z.; Dickey, E.C.; LeBeau, J.M.; Wang, J.; Luo, J.; Taylor, S.; Hackenberger, W.; et al. Giant piezoelectricity of Sm-doped $Pb(Mg_{1/3}Nb_{2/3})O_3$-$PbTiO_3$ single crystals. *Science* **2019**, *364*, 264–268. [CrossRef] [PubMed]
25. Xu, G.; Chen, K.; Yang, D.; Li, J. Growth and electrical properties of large size $Pb(In_{1/2}Nb_{1/2})O_3$-$Pb(Mg_{1/3}Nb_{2/3})O_3$-$PbTiO_3$ crystals prepared by the vertical Bridgman technique. *Appl. Phys. Lett.* **2007**, *90*, 032901. [CrossRef]
26. Swartz, S.L.; Shrout, T.R. Fabrication of perovskite lead magnesium niobate. *Mater. Res. Bull.* **1982**, *17*, 1245–1250. [CrossRef]
27. Cao, W. Full-set material properties and domain engineering principles of ferroelectric single crystals. In *Handbook of Advanced Dielectric, Piezoelectric and Ferroelectric Materials*; Ye, Z.G., Ed.; Woodhead: Cambridge, UK, 2008; pp. 235–265.
28. Song, K.; Li, Z.; Guo, H.; Xu, Z.; Fan, S. Compositional segregation and electrical properties characterization of [001]-and [011]-oriented co-growth $Pb(In_{1/2}Nb_{1/2})O_3$-$Pb(Mg_{1/3}Nb_{2/3})O_3$-$PbTiO_3$ single crystal. *J. Appl. Phys.* **2018**, *123*, 154107. [CrossRef]
29. Li, F.; Zhang, S.; Xu, Z.; Wei, X.; Luo, J.; Shrout, T.R. Composition and phase dependence of the intrinsic and extrinsic piezoelectric activity of domain engineered $Pb(Mg_{1/3}Nb_{2/3})O_3$-$PbTiO_3$ crystals. *J. Appl. Phys.* **2010**, *108*, 034106. [CrossRef] [PubMed]
30. Feng, Z.; Zhao, X.; Luo, H. Composition and orientation dependence of dielectric and piezoelectric properties in poled $Pb(Mg_{1/3}Nb_{2/3})O_3$-$PbTiO_3$ crystals. *J. Appl. Phys.* **2006**, *100*, 024104. [CrossRef]
31. Zhang, S.; Lee, S.M.; Kim, D.H.; Lee, H.Y.; Shrout, T.R. Elastic, piezoelectric, and dielectric properties of $0.71Pb(Mg_{1/3}Nb_{2/3})O_3$-$0.29PbTiO_3$ crystals obtained by solid-state crystal growth. *J. Am. Ceram. Soc.* **2008**, *91*, 683–686. [CrossRef]
32. Han, J.; Cao, W. Electric field effects on the phase transitions in [001]-oriented $(1-x)Pb(Mg_{1/3}Nb_{2/3})O_3-xPbTiO_3$ single crystals with compositions near the morphotropic phase boundary. *Phys. Rev. B* **2003**, *68*, 134102. [CrossRef]
33. Luo, C.; Karaki, T.; Sun, Y.; Yamashita, Y.J.; Xu, J. Effect of field cooling AC poling on electrical and physical properties for $Pb(Mg_{1/3}Nb_{2/3})O_3$-$PbTiO_3$-based single crystals manufactured by a continuous-feeding Bridgman process. *Jpn. J. Appl. Phys.* **2020**, *59*, SPPD07. [CrossRef]
34. Sun, E.; Zhang, R.; Wu, F.; Yang, B.; Cao, W. Influence of manganese doping to the full tensor properties of $0.24Pb(In_{1/2}Nb_{1/2})O_3$-$0.47Pb(Mg_{1/3}Nb_{2/3})O_3$-$0.29PbTiO_3$ single crystals. *J. Appl. Phys.* **2013**, *113*, 074108. [CrossRef]
35. Huo, X.; Zhang, S.; Liu, G.; Zhang, R.; Luo, J.; Sahul, R.; Cao, W.; Shrout, T.R. Elastic, dielectric and piezoelectric characterization of single domain PIN-PMN-PT:Mn crystals. *J. Appl. Phys.* **2012**, *112*, 124113. [CrossRef]
36. Kong, L.; Liu, G.; Zhang, S.; Liu, H. The role of tetragonal side morphotropic phase boundary in modified relaxor-$PbTiO_3$ crystals for high power transducer applications. *J. Appl. Phys.* **2013**, *114*, 144106. [CrossRef]
37. Li, F.; Zhang, S.; Xu, Z.; Wei, X.; Luo, J.; Shrout, T.R. Electromechanical properties of tetragonal $Pb(In_{1/2}Nb_{1/2})O_3-Pb(Mg_{1/3}Nb_{2/3})O_3-PbTiO_3$ ferroelectric crystals. *J. Appl. Phys.* **2010**, *107*, 054107. [CrossRef] [PubMed]
38. Jing, Y.; Zheng, L.; Lü, W.; Xi, Z.; Zheng, P.; Du, J.; Zhang, R. Full tensor properties of single-domain tetragonal $0.63Pb(Mg_{1/3}Nb_{2/3})O_3$-0.37PbTiO3 single crystal and their orientation dependence. *Phys. Status Solidi B* **2016**, *253*, 1994–2000. [CrossRef]
39. Zhang, R.; Jiang, B.; Cao, W. Elastic, piezoelectric, and dielectric properties of multidomain $0.67Pb(Mg_{1/3}Nb_{2/3})O_3$–$0.33PbTiO_3$ single crystals. *J. Appl. Phys.* **2001**, *90*, 3471–3475. [CrossRef]
40. Li, F.; Jin, L.; Xu, Z.; Wang, D.; Zhang, S. Electrostrictive effect in $Pb(Mg_{1/3}Nb_{2/3})O_3$-$xPbTiO_3$ crystals. *Appl. Phys. Lett.* **2013**, *102*, 152910.
41. Zhang, S.; Sherlock, N.P.; Meyer, R.J., Jr.; Shrout, T.R. Crystallographic dependence of loss in domain engineered relaxor-PT single crystals. *Appl. Phys. Lett.* **2009**, *94*, 162906. [CrossRef]
42. Li, F.; Zhang, S.; Xu, Z.; Wei, X.; Luo, J.; Shrout, T.R. Temperature independent shear piezoelectric response in relaxor-$PbTiO_3$ based crystals. *Appl. Phys. Lett.* **2010**, *97*, 252903. [CrossRef]
43. Bridgman, P.W. Certain physical properties of single crystals of tungsten, antimony, bismuth, tellurium, cadmium, zinc, and tin. *Proc. Am. Acad. Arts Sci. USA* **1925**, *60*, 305. [CrossRef]
44. Stockbarger, D.C. The production of large single crystals of lithium fluoride. *Rev. Sci. Instrum.* **1936**, *7*, 133–136. [CrossRef]
45. Han, P.; Tian, J.; Yan, W. Bridgman growth and properties of PMN-PT-based single crystals. In *Handbook of Advanced Dielectric, Piezoelectric and Ferroelectric Materials: Synthesis, Properties and Applications*; Ye, Z.G., Ed.; Woodhead: Cambridge, UK, 2008; pp. 3–37.

46. Hackenberger, W.; Luo, J.; Jiang, X.N.; Snook, K.A.; Rehrig, P.W.; Zhang, S.J.; Shrout, T.R. Recent developments and applications of piezoelectric crystals. In *Handbook of Advanced Dielectric, Piezoelectric and Ferroelectric Materials–Synthesis, Characterization and Applications*; Ye, Z.G., Ed.; Woodhead: Cambridge, UK, 2008; pp. 73–100.
47. Luo, J.; Zhang, S. Advances in the growth and characterization of relaxor-PT-based ferroelectric single crystals. *Crystals* **2014**, *4*, 306–330. [CrossRef]
48. Luo, H.; Xu, G.; Xu, H.; Wang, P.; Yin, Z. Compositional homogeneity and electrical properties of lead magnesium niobate titanate single crystals grown by a modified Bridgman technique. *Jpn. J. Appl. Phys.* **2000**, *39*, 5581. [CrossRef]
49. Zawilski, K.T.; Custodio, M.C.C.; DeMattei, R.C.; Lee, S.G.; Monteiro, R.G.; Odagawa, H.; Feigelson, R.S. Segregation during the vertical Bridgman growth of lead magnesium niobate–lead titanate single crystals. *J. Cryst. Growth* **2003**, *258*, 353–367. [CrossRef]
50. Zhang, W.; Wang, Z.; Yang, X.; Long, X.; He, C. Composition uniformity of $Pb(In_{1/2}Nb_{1/2})O_3$-Pb $(Mg_{1/3}Nb_{2/3})O_3$-$PbTiO_3$ single crystals grown in ⟨001⟩ direction. *J. Cryst. Growth* **2021**, *560*, 126061. [CrossRef]
51. Zawilski, K.T.; DeMattei, R.C.; Feigelson, R.S. Zone leveling of lead magnesium niobate–lead titanate crystals using RF heating. *J. Cryst. Growth* **2005**, *277*, 393–400. [CrossRef]
52. Echizenya, K.; Matsushita, M. Continuous feed growth and characterization of PMN-PT single crystals. In Proceedings of the 2011 IEEE International Ultrasonics Symposium, Orlando, FL, USA, 18–21 October 2011; pp. 1813–1816.
53. Matsushitata, M.; Echizenya, K. Continuous feeding growth of ternary PIN-PMN-PT single crystals. In Proceedings of the 2014 Joint IEEE International Symposium on the Applications of Ferroelectric, International Workshop on Acoustic Transduction Materials and Devices & Workshop on Piezoresponse Force Microscopy, University Park, PA, USA, 12–16 May 2014; pp. 1–4.
54. Echizenya, K.; Nakamura, K.; Mizuno, K. PMN-PT and PIN-PMN-PT single crystals grown by continuous-feeding Bridgman method. *J. Cryst. Growth* **2020**, *531*, 125364. [CrossRef]
55. Li, Z.; Song, K.; Guo, H.; Liu, Y.; Ma, M.; Fan, S.; Xu, Z. High composition uniformity of 4″ of PIN-PMN-PT single crystals grown by the modified Bridgman method. *J. Cryst. Growth* **2017**, *468*, 331–334. [CrossRef]
56. Song, K.; Li, Q.; Guo, H.; Hu, Q.; Li, Z.; Li, F.; Fan, S.; Xu, Z. Composition and electrical properties characterization of a 5″ diameter PIN-PMN-PT single crystal by the modified Bridgman method. *J. Alloys Compd.* **2021**, *851*, 156145. [CrossRef]
57. Lee, H.Y. Development of high-performance piezoelectric single crystals by using solid-state single crystal growth (SSCG) method. In *Handbook of Advanced Dielectric, Piezoelectric and Ferroelectric Materials*; Ye, Z.G., Ed.; Woodhead: Cambridge, UK, 2008; pp. 158–172.
58. Kabakov, P.; Dean, C.; Kurusingal, V.; Cheng, Z.; Lee, H.Y.; Zhang, S. Solid-state crystal growth of lead-free ferroelectrics. *J. Mater. Chem. C* **2020**, *8*, 7606–7649. [CrossRef]
59. Zhang, S.; Lee, S.M.; Kim, D.H.; Lee, H.Y.; Shrout, T.R. Electromechanical properties of PMN–PZT piezoelectric single crystals near morphotropic phase boundary compositions. *J. Am. Ceram. Soc.* **2007**, *90*, 3859–3862. [CrossRef]
60. Kang, S.J.L.; Park, J.H.; Ko, S.Y.; Lee, H.Y. Solid-state conversion of single crystals: The principle and the state-of-the-art. *J. Am. Ceram. Soc.* **2015**, *98*, 347–360. [CrossRef]
61. Kang, S.J.L.; Ko, S.Y.; Moon, S.Y. Mixed control of boundary migration and the principle of microstructural evolution. *J. Ceram. Soc. Jpn.* **2016**, *124*, 259–267. [CrossRef]
62. Yamamoto, T.; Sakuma, T. Fabrication of barium titanate single crystals by solid-state grain growth. *J. Am. Ceram. Soc.* **1994**, *77*, 1107–1109. [CrossRef]
63. Yoo, Y.S.; Kang, M.K.; Han, J.H.; Kim, H.; Kim, D.Y. Fabrication of $BaTiO_3$ single crystals by using the exaggerated grain growth method. *J. Eur. Ceram. Soc.* **1997**, *17*, 1725–1727. [CrossRef]
64. Rehrig, P.W.; Messing, G.L.; Trolier-McKinstry, S. Templated grain growth of barium titanate single crystals. *J. Am. Ceram. Soc.* **2000**, *83*, 2654–2660. [CrossRef]
65. Lee, H.Y.; Kim, J.S.; Kim, D.Y. Fabrication of $BaTiO_3$ single crystals using secondary abnormal grain growth. *J. Eur. Ceram. Soc.* **2000**, *20*, 1595–1597. [CrossRef]
66. Li, T.; Scotch, A.M.; Chan, H.M.; Harmer, M.P.; Park, S.E.; Shrout, T.R.; Michael, J.R. Single crystals of $Pb(Mg_{1/3}Nb_{2/3})O_3$—35mol%$PbTiO_3$ from polycrystalline precursors. *J. Am. Ceram. Soc.* **1998**, *81*, 244–248. [CrossRef]
67. Chen, Z.; Liao, X.; Chen, J.; Zhang, S. The visible hand behind properties. *Microstructures* **2021**, *1*, 2021001. [CrossRef]
68. Kim, M.S.; Fisher, J.G.; Kang, S.J.L.; Lee, H.Y. Grain growth control and solid-state crystal growth by Li_2O/PbO addition and dislocation introduction in the PMN-35PT system. *J. Am. Ceram. Soc.* **2006**, *89*, 1237–1243. [CrossRef]
69. Lim, J.B.; Zhang, S.; Lee, H.Y.; Shrout, T.R. Solid state crystal growth of $BiScO_3$-$Pb(Mg_{1/3}Nb_{2/3})O_3$-$PbTiO_3$. *J. Electroceram.* **2012**, *29*, 139–143. [CrossRef]
70. King, P.T.; Gorzkowski, E.P.; Scotch, A.M.; Rockosi, D.J.; Chan, H.M.; Harmer, M.P. Kinetics of {001} $Pb(Mg_{1/3}Nb_{2/3})O_3$–35mol%$PbTiO_3$ single crystals grown by seeded polycrystal conversion. *J. Am. Ceram. Soc.* **2003**, *86*, 2182–2187. [CrossRef]
71. Khan, A.; Meschke, F.A.; Li, T.; Scotch, A.M.; Chan, H.M.; Harmer, M.P. Growth of $Pb(Mg_{1/3}Nb_{2/3})O_3$-35mol% $PbTiO_3$ single crystals from (111) substrates by seeded polycrystal conversion. *J. Am. Ceram. Soc.* **1999**, *82*, 2958–2962. [CrossRef]
72. Khan, A.; Gorzkowski, E.P.; Scotch, A.M.; Leite, E.R.; Li, T.; Chan, H.M.; Harmer, M.P. Influence of excess PbO additions on {111} single-grystal growth of $Pb(Mg_{1/3}Nb_{2/3})O_3$-35mol%$PbTiO_3$ by seeded polycrystal conversion. *J. Am. Ceram. Soc.* **2003**, *86*, 2176–2181. [CrossRef]
73. Liu, G.; Kong, L.; Hu, Q.; Zhang, S. Diffused morphotropic phase boundary in relaxor-$PbTiO_3$ crystals: High piezoelectricity with improved thermal stability. *Appl. Phys. Rev.* **2020**, *7*, 021405. [CrossRef]

74. Li, F.; Zhang, S.; Yang, T.; Xu, Z.; Zhang, N.; Liu, G.; Wang, J.; Wang, J.; Cheng, Z.; Ye, Z.G.; et al. The origin of ultrahigh piezoelectricity in relaxor-ferroelectric solid solution crystals. *Nat. Commun.* **2016**, *7*, 1–9. [CrossRef]
75. Bell, A.J. Phenomenologically derived electric field-temperature phase diagrams and piezoelectric coefficients for single crystal barium titanate under fields along different axes. *J. Appl. Phys.* **2001**, *89*, 3907–3914. [CrossRef]
76. Feng, Z.; Zhao, X.; Luo, H. Effect of poling field and temperature on dielectric and piezoelectric property of ⟨001⟩-oriented $0.70Pb(Mg_{1/3}Nb_{2/3})O_3$–$0.30PbTiO_3$ crystals. *Mater. Res. Bull.* **2006**, *41*, 1133–1137. [CrossRef]
77. Davis, M. Phase Transitions, Anisotropy and Domain Engineering: The Piezoelectric Properties of Relaxor-Ferroelectric Single Crystals. Doctoral Thesis, EPFL, Lausanne, Switzerland, 2006.
78. Guo, Y.; Luo, H.; Ling, D.; Xu, H.; He, T.; Yin, Z. The phase transition sequence and the location of the morphotropic phase boundary region in $(1-x)[Pb(Mg_{1/3}Nb_{2/3})O_3]$–$xPbTiO_3$ single crystal. *J. Condens. Matter Phys.* **2003**, *15*, L77. [CrossRef]
79. Shanthi, M.; Hoe, K.H.; Lim, C.Y.H.; Lim, L.C. Overpoling-induced property degradation in $Pb(Mg_{1/3}Nb_{2/3})O_3$-$PbTiO_3$ single crystals of near-morphotropic phase boundary compositions. *Appl. Phys. Lett.* **2005**, *86*, 262908.
80. Bokov, A.A.; Ye, Z.G. Field-induced shift of morphotropic phase boundary and effect of overpoling in $(1-x)Pb(Mg_{1/3}Nb_{2/3})O_3$–$xPbTiO_3$ piezocrystals. *Appl. Phys. Lett.* **2008**, *92*, 082901. [CrossRef]
81. Tu, C.S.; Chien, R.R.; Lee, S.C.; Schmidt, V.H.; Luo, H. Rapid piezoelectric response and origin in $(001)Pb(In_{1/2}Nb_{1/2})_{0.70}Ti_{0.30}O_3$ crystal. *J. Appl. Phys.* **2009**, *106*, 016102. [CrossRef]
82. Tu, C.S.; Hsieh, C.M.; Schmidt, V.H.; Chien, R.R.; Luo, H. Piezoelectric response and origin in $(001)Pb(Mg_{1/3}Nb_{2/3})_{0.70}Ti_{0.30}O_3$ crystal. *Appl. Phys. Lett.* **2008**, *93*, 172905. [CrossRef]
83. Jiang, Z. Over-poling study of PMN-PT and PIN-PMN-PT crystal grown by Vertical Gradient Freeze method. In Proceedings of the 2016 Joint IEEE International Symposium on the Applications of Ferroelectrics, European Conference on Application of Polar Dielectrics, and Piezoelectric Force Microscopy Workshop (ISAF/ECAPD/PFM), Darmstadt, Germany, 21–25 August 2016; pp. 1–4.
84. Yamamoto, N.; Yamashita, Y.; Itsumi, K.; Hosono, Y. Temperature dependence of dielectric constant with different poling fields in lead magnesium niobate-lead titanate single crystal. *Trans. Mater. Res. Soc. Jpn.* **2010**, *35*, 95–98. [CrossRef]
85. Chen, H.Y.; Tu, C.S.; Hung, C.M.; Chien, R.R.; Schmidt, V.H.; Ku, C.S.; Lee, H.Y. Poling effect and piezoelectric response in high-strain ferroelectric $0.70Pb(Mg_{1/3}Nb_{2/3})O_3$–$0.30\ PbTiO_3$ crystal. *J. Appl. Phys.* **2010**, *108*, 044101. [CrossRef]
86. Lin, D.; Li, Z.; Zhang, S.; Xu, Z.; Yao, X. Electric-field and temperature induced phase transitions in $Pb(Mg_{1/3}Nb_{2/3})O_3$–$0.3PbTiO_3$ single crystals. *J. Appl. Phys.* **2010**, *108*, 034112. [CrossRef]
87. Chen, Z.; Hong, L.; Wang, F.; Ringer, S.P.; Chen, L.Q.; Luo, H.; Liao, X. Facilitation of ferroelectric switching via mechanical manipulation of hierarchical nanoscale domain structures. *Phys. Rev. Lett.* **2017**, *118*, 017601. [CrossRef]
88. Chen, Z.; Hong, L.; Wang, F.; An, X.; Wang, X.; Ringer, S.; Chen, L.Q.; Luo, H.; Liao, X. Kinetics of domain switching by mechanical and electrical stimulation in relaxor-based ferroelectrics. *Phys. Rev. Appl.* **2017**, *8*, 064005. [CrossRef]
89. Chen, Z.; Li, F.; Huang, Q.; Liu, F.; Wang, F.; Ringer, S.P.; Luo, H.; Zhang, S.; Chen, L.Q.; Liao, X. Giant tuning of ferroelectricity in single crystals by thickness engineering. *Sci. Adv.* **2020**, *6*, eabc7156. [CrossRef]
90. Huang, Q.; Chen, Z.; Cabral, M.J.; Wang, F.; Zhang, S.; Li, F.; Li, Y.; Ringer, S.P.; Luo, H.; Mai, Y.W.; et al. Direct observation of nanoscale dynamics of ferroelectric degradation. *Nat. Commun.* **2021**, *12*, 1–7. [CrossRef]
91. Noheda, B.; Zhong, Z.; Cox, D.E.; Shirane, G.; Park, S.E.; Rehrig, P. Electric-field-induced phase transitions in rhombohedral $Pb(Zn_{1/3}Nb_{2/3})_{1-x}Ti_xO_3$. *Phys. Rev. B* **2002**, *65*, 224101. [CrossRef]
92. Bai, F.; Wang, N.; Li, J.; Viehland, D.; Gehring, P.M.; Xu, G.; Shirane, G. X-ray and neutron diffraction investigations of the structural phase transformation sequence under electric field in $0.7Pb(Mg_{1/3}Nb_{2/3})$-$0.3PbTiO_3$ crystal. *J. Appl. Phys.* **2004**, *96*, 1620–1627. [CrossRef]
93. Wang, Y.; Wang, D.; Yuan, G.; Ma, H.; Xu, F.; Li, J.; Viehland, D.; Gehring, P.M. Fragile morphotropic phase boundary and phase stability in the near-surface region of the relaxor ferroelectric $(1-x)Pb(Zn_{1/3}Nb_{2/3})O_3-xPbTiO_3$:[001] field-cooled phase diagrams. *Phys. Rev. B* **2016**, *94*, 174103. [CrossRef]
94. Li, F.; Wang, L.; Jin, L.; Xu, Z.; Zhang, S. Achieving single domain relaxor-PT crystals by high temperature poling. *CrystEngComm* **2014**, *16*, 2892–2897. [CrossRef]
95. Hu, W.; Xi, Z.; Fang, P.; Long, W.; Li, X.; Bu, Q. A novel poling technique to obtain excellent piezoelectric properties of $Pb(Mg_{1/3}Nb_{2/3})O_3$–$0.32PbTiO_3$ single crystals. *J. Mater. Sci. Mater. Electron.* **2015**, *26*, 3282–3286. [CrossRef]
96. Li, F.; Zhang, S.; Xu, Z.; Li, Z.; Wei, X. DC bias electric field dependent piezoelectricity for [001] poled $Pb(In_{1/2}Nb_{1/2})O_3$–$Pb(Mg_{1/3}Nb_{2/3})\ O_3$–$PbTiO_3$ crystals. *J. Adv. Dielectr.* **2011**, *1*, 303–308. [CrossRef]
97. Lin, D.; Zhang, S.; Li, Z.; Li, F.; Xu, Z.; Wada, S.; Luo, J.; Shrout, T.R. Domain size engineering in tetragonal $Pb(In_{1/2}Nb_{1/2})O_3$-$Pb(Mg_{1/3}Nb_{2/3})O_3$-$PbTiO_3$ crystals. *J. Appl. Phys.* **2011**, *110*, 084110. [CrossRef]
98. Shen, Z.Y.; Tang, Y.; Zhang, S.; Luo, J.; Li, Y.; Shrout, T.R. Enhanced piezoelectric activity and temperature stability of [111]-oriented orthorhombic $0.68Pb(Mg_{1/3}Nb_{2/3})O_3$–$0.32PbTiO_3$ single crystals by domain size engineering. *Scr. Mater.* **2014**, *72*, 17–20. [CrossRef]
99. Zhao, Y.; Wang, S.; Fu, X.; Zhuang, Y.; Yang, R.; Yang, Z.; Li, Z.; Xu, Z.; Wei, X. Thermal annealing and single–domain preparation in tetragonal $Pb(In_{1/2}Nb_{1/2})O_3$-$Pb(Mg_{1/3}Nb_{2/3})O_3$–$PbTiO_3$ crystal for electro–optic and non–linear optical applications. *J. Appl. Phys.* **2018**, *123*, 084104. [CrossRef]

100. Xu, J.; Deng, H.; Zeng, Z.; Zhang, Z.; Zhao, K.; Chen, J.; Nakamori, N.; Wang, F.; Ma, J.; Li, X.; et al. Piezoelectric performance enhancement of $Pb(Mg_{1/3}Nb_{2/3})O_3$-0.25$PbTiO_3$ crystals by alternating current polarization for ultrasonic transducer. *Appl. Phys. Lett.* **2018**, *112*, 182901. [CrossRef]
101. Luo, C.; Karaki, T.; Wang, Z.; Sun, Y.; Yamashita, Y.; Xu, J. High piezoelectricity after field cooling AC poling in ferroelectric crystals manufactured by continuous-feeding Bridgman. *J. Adv. Ceram.* **2021**, *11*, 57–65. [CrossRef]
102. Wan, H.; Luo, C.; Chung, C.C.; Yamashita, Y.; Jiang, X. Enhanced dielectric and piezoelectric properties of manganese-doped $Pb(In_{1/2}Nb_{1/2})O_3$-Pb $(Mg_{1/3}Nb_{2/3})O_3$-$PbTiO_3$ single crystals by alternating current poling. *Appl. Phys. Lett.* **2021**, *118*, 102904. [CrossRef]
103. Sun, Y.; Karaki, T.; Fujii, T.; Yamashita, Y. Alternate current poling and direct current poling for $Pb(Mg_{1/3}Nb_{2/3})O_3$–$PbTiO_3$ single crystals. *Jpn. J. Appl. Phys.* **2019**, *58*, SLLC06. [CrossRef]
104. Ma, M.; Xia, S.; Song, K.; Guo, H.; Fan, S.; Li, Z. Enhanced dielectric and piezoelectric properties in the [001]-poled 0.25$Pb(In_{1/2}Nb_{1/2})O_3$-0.43$Pb(Mg_{1/3}Nb_{2/3})O_3$-0.32$PbTiO_3$ single crystal near morphotropic phase boundary by alternating current treatment. *J. Appl. Phys.* **2020**, *127*, 064106. [CrossRef]
105. Guo, L.; Su, B.; Wang, C.; He, X.; Wang, Z.; Yang, X.; Long, X.; He, C. Orientation dependence of dielectric and piezoelectric properties of tetragonal relaxor ferroelectric single crystals by alternate current poling. *J. Appl. Phys.* **2020**, *127*, 184104. [CrossRef]
106. He, C.; Karaki, T.; Yang, X.; Yamashita, Y.J.; Sun, Y.; Long, X. Dielectric and piezoelectric properties of $Pb[(Mg_{1/3}Nb_{2/3})0.52(Yb_{1/2}Nb_{1/2})0.15Ti_{0.33}]O_3$ single-crystal rectangular plate and beam mode transducers poled by alternate current poling. *Jpn. J. Appl. Phys.* **2019**, *58*, SLLD06. [CrossRef]
107. Vanderbilt, D.; Cohen, M.H. Monoclinic and triclinic phases in higher-order Devonshire theory. *Phys. Rev. B* **2001**, *63*, 094108. [CrossRef]
108. Noheda, B.; Cox, D.E.; Shirane, G.; Park, S.E.; Cross, L.E.; Zhong, Z. Polarization rotation via a monoclinic phase in the piezoelectric 92%$PbZn_{1/3}Nb_{2/3}O_3$-8%$PbTiO_3$. *Phys. Rev. Lett.* **2001**, *86*, 3891. [CrossRef]
109. Qiu, C.; Wang, B.; Zhang, N.; Zhang, S.; Liu, J.; Walker, D.; Wang, Y.; Tian, H.; Shrout, T.R.; Xu, Z.; et al. Transparent ferroelectric crystals with ultrahigh piezoelectricity. *Nature* **2020**, *577*, 350–354. [CrossRef] [PubMed]
110. Qiu, C.; Xu, Z.; An, Z.; Liu, J.; Zhang, G.; Zhang, S.; Chen, L.Q.; Zhang, N.; Li, F. In-situ domain structure characterization of $Pb(Mg_{1/3}Nb_{2/3})O_3$-$PbTiO_3$ crystals under alternating current electric field poling. *Acta Mater.* **2021**, *210*, 116853. [CrossRef]
111. Wan, H.; Luo, C.; Liu, C.; Chang, W.Y.; Yamashita, Y.; Jiang, X. Alternating current poling on sliver-mode rhombohedral $Pb(Mg_{1/3}Nb_{2/3)}O_3$-$PbTiO_3$ single crystals. *Acta Mater.* **2021**, *208*, 116759. [CrossRef]
112. Liu, J.; Qiu, C.; Qiao, L.; Song, K.; Guo, H.; Xu, Z.; Li, F. Impact of alternating current electric field poling on piezoelectric and dielectric properties of $Pb(In_{1/2}Nb_{1/2})O_3$–$Pb(Mg_{1/3}Nb_{2/3})O_3$–$PbTiO_3$ ferroelectric crystals. *J. Appl. Phys.* **2020**, *128*, 094104. [CrossRef]
113. Wang, B.; Li, F.; Chen, L.Q. Inverse domain-size dependence of piezoelectricity in ferroelectric crystals. *Adv. Mater.* **2021**, *33*, 2105071. [CrossRef]
114. Ma, M.; Xia, S.; Song, K.; Guo, H.; Xu, Z.; Li, Z. Temperature dependence of the transverse piezoelectric properties in the [001]-poled 0.25$Pb(In_{1/2}Nb_{1/2})O_3$-0.42$Pb(Mg_{1/3}Nb_{2/3})O_3$-0.33$PbTiO_3$ single crystal with alternating current treatment. *J. Appl. Phys.* **2021**, *129*, 114102. [CrossRef]
115. Deng, T.; Fang, B.; Chen, Z.; Chen, J.; Luo, H. Improving fatigue resistance of PIMNT single crystal via two-step poling process. *J. Phys. Chem. Solids* **2022**, *161*, 110378. [CrossRef]
116. Sun, Y.; Karaki, T.; Fujii, T.; Yamashita, Y.J. Spurious-mode vibrations caused by alternating current poling and their solution process for $Pb(Mg_{1/3}Nb_{2/3})O_3$-$PbTiO_3$ single crystals. *J. Mater.* **2021**, in press. [CrossRef]
117. Luo, C.; Karaki, T.; Yamashita, Y.J.; Xu, J. High temperature and low voltage AC poling for 0.24$Pb(In_{1/2}Nb_{1/2})O_3$-0.46$Pb(Mg_{1/3}Nb_{2/3})O_3$-0.30$PbTiO_3$ piezoelectric single crystals manufactured by continuous-feeding Bridgman method. *J. Mater.* **2021**, *7*, 621–628. [CrossRef]
118. Wan, H.; Luo, C.; Chang, W.Y.; Yamashita, Y.; Jiang, X. Effect of poling temperature on piezoelectric and dielectric properties of 0.7$Pb(Mg_{1/3}Nb_{2/3})O_3$-0.3PbTiO3 single crystals under alternating current poling. *Appl. Phys. Lett.* **2019**, *114*, 172901. [CrossRef]
119. Luo, C.; Wan, H.; Chang, W.Y.; Yamashita, Y.; Paterson, A.R.; Jones, J.; Jiang, X. Effect of low-frequency alternating current poling on 5-mm-thick 0.7$Pb(Mg_{1/3}Nb_{2/3})O_3$-0.3$PbTiO_3$ single crystals. *Appl. Phys. Lett.* **2019**, *115*, 192904. [CrossRef]
120. Sun, Y.; Karaki, T.; Fujii, T.; Yamashita, Y. Enhanced electric property of relaxor ferroelectric crystals with low AC voltage high-temperature poling. *Jpn. J. Appl. Phys.* **2020**, *59*, SPPD08. [CrossRef]
121. Jiang, H.; Zou, Y.K.; Chen, Q.; Li, K.K.; Zhang, R.; Wang, Y.; Ming, H.; Zheng, Z. Transparent electro-optic ceramics and devices. *Proc. SPIE* **2005**, *5644*, 380–394.
122. Fang, Z.; Jiang, X.; Tian, X.; Zheng, F.; Cheng, M.; Zhao, E.; Ye, W.; Qin, Y.; Zhang, Y. Ultratransparent PMN-PT electro-optic ceramics and its application in optical communication. *Adv. Opt. Mater.* **2021**, *9*, 2002139. [CrossRef]
123. Berlincourt, D. Piezoelectric ceramic compositional development. *J. Acoust. Soc. Am.* **1992**, *91*, 3034–3040. [CrossRef]
124. Luo, N.; Zhang, S.; Li, Q.; Yan, Q.; Zhang, Y.; Ansell, T.; Luo, J.; Shrout, T.R. Crystallographic dependence of internal bias in domain engineered Mn-doped relaxor-$PbTiO_3$ single crystals. *J. Mater. Chem. C* **2016**, *4*, 4568–4576. [CrossRef]
125. Sherlock, N.P.; Zhang, S.; Luo, J.; Lee, H.Y.; Shrout, T.R.; Meyer, R.J., Jr. Large signal electromechanical properties of low loss $(1-x)Pb(Mg_{1/3}Nb_{2/3})O_3-xPbTiO_3$ single crystals. *J. Appl. Phys.* **2010**, *107*, 074108. [CrossRef]

126. Moffett, M.B.; Robinson, H.C.; Powers, J.M.; Baird, P.D. Single-crystal lead magnesium niobate-lead titanate (PMN/PT) as a broadband high power transduction material. *J. Acoust. Soc. Am.* **2007**, *121*, 2591–2599. [CrossRef]
127. Chen, Y.H.; Uchino, K.; Shen, M.; Viehland, D. Substituent effects on the mechanical quality factor of $Pb(Mg_{1/3}Nb_{2/3})O_3$–$PbTiO_3$ and $Pb(Sc_{1/2}Nb_{1/2})O_3$–$PbTiO_3$ ceramics. *J. Appl. Phys.* **2001**, *90*, 1455–1458. [CrossRef]
128. Zhang, S.; Lebrun, L.; Randall, C.A.; Shrout, T.R. Orientation dependence properties of modified tetragonal $0.88Pb(Zn_{1/3}Nb_{2/3})O_3$–$0.12PbTiO_3$ single crystals. *Phys. Status Solidi A* **2005**, *202*, 151–157. [CrossRef]
129. Qiao, H.; He, C.; Wang, Z.; Pang, D.; Li, X.; Liu, Y.; Long, X. Influence of Mn dopants on the electrical properties of $Pb(In_{0.5}Nb_{0.5})O_3$–$PbTiO_3$ ferroelectric single crystals. *RSC Adv.* **2017**, *7*, 32607–32612. [CrossRef]
130. Huo, X.; Zhang, S.; Liu, G.; Zhang, R.; Luo, J.; Sahul, R.; Cao, W.; Shrout, T.R. Complete set of elastic, dielectric, and piezoelectric constants of $[011]_C$ poled rhombohedral $Pb(In_{0.5}Nb_{0.5})O_3$-$Pb(Mg_{1/3}Nb_{2/3})O_3$-$PbTiO_3$:Mn single crystals. *J. Appl. Phys.* **2013**, *113*, 074106. [CrossRef]
131. Zheng, L.; Sahul, R.; Zhang, S.; Jiang, W.; Li, S.; Cao, W. Orientation dependence of piezoelectric properties and mechanical quality factors of $0.27Pb(In_{1/2}Nb_{1/2})O_3$-$0.46Pb(Mg_{1/3}Nb_{2/3})O_3$-$0.27PbTiO_3$:Mn single crystals. *J. Appl. Phys.* **2013**, *114*, 104105. [CrossRef]
132. Zhang, S.; Xia, R.; Lebrun, L.; Anderson, D.; Shrout, T.R. Piezoelectric materials for high power, high temperature applications. *Mater. Lett.* **2005**, *59*, 3471–3475. [CrossRef]
133. Sun, E.; Zhang, S.; Luo, J.; Shrout, T.R.; Cao, W. Elastic, dielectric, and piezoelectric constants of $Pb(In_{1/2}Nb_{1/2})O_3$–$Pb(Mg_{1/3}Nb_{2/3})O_3$–$PbTiO_3$ single crystal poled along $[011]_c$. *Appl. Phys. Lett.* **2010**, *97*, 032902. [CrossRef] [PubMed]
134. Zhang, S.; Taylor, S.; Li, F.; Luo, J.; Meyer, R.J., Jr. Piezoelectric property of relaxor-$PbTiO_3$ crystals under uniaxial transverse stress. *Appl. Phys. Lett.* **2013**, *102*, 172902. [CrossRef]
135. Liu, G.; Zhang, S.; Jiang, W.; Cao, W. Losses in ferroelectric materials. *Mater. Sci. Eng. R Rep.* **2015**, *89*, 1–48. [CrossRef] [PubMed]
136. Rhim, S.M.; Shin, M.C.; Lee, S.G. Piezoelectric single crystals for medical ultrasonic transducers. In *Handbook of Advanced Dielectric, Piezoelectric and Ferroelectric Materials*; Ye, Z.G., Ed.; Woodhead Publishing: Cambridge, UK, 2008; pp. 101–129.
137. Viehland, D.; Li, J.F.; Jang, S.J.; Cross, L.E.; Wuttig, M. Glassy polarization behavior of relaxor ferroelectrics. *Phys. Rev. B* **1992**, *46*, 8013. [CrossRef]
138. Haertling, G.H. Ferroelectric ceramics: History and technology. *J. Am. Ceram. Soc.* **1999**, *82*, 797–818. [CrossRef]
139. Dai, X.; DiGiovanni, A.; Viehland, D. Dielectric properties of tetragonal lanthanum modified lead zirconate titanate ceramics. *J. Appl. Phys.* **1993**, *74*, 3399–3405. [CrossRef]
140. Samara, G.A. The relaxational properties of compositionally disordered ABO_3 perovskites. *J. Condens. Matter Phys.* **2003**, *15*, R367. [CrossRef]
141. Liu, Y.; Ling, Z.; Zhuo, Z. High piezoelectricity of PLZT ceramics with strong frequency-dielectric dispersion below depolarization temperature. *J. Alloys Compd.* **2017**, *727*, 925–930. [CrossRef]
142. Seshadri, S.B.; Nolan, M.M.; Tutuncu, G.; Forrester, J.S.; Sapper, E.; Esteves, G.; Granzow, T.; Thomas, P.A.; Nino, J.C.; Rojac, T.; et al. Unexpectedly high piezoelectricity of Sm-doped lead zirconate titanate in the Curie point region. *Sci. Rep.* **2018**, *8*, 1–13. [CrossRef] [PubMed]
143. Gao, B.; Yao, Z.; Lai, D.; Guo, Q.; Pan, W.; Hao, H.; Cao, M.; Liu, H. Unexpectedly high piezoelectric response in Sm-doped PZT ceramics beyond the morphotropic phase boundary region. *J. Alloys Compd.* **2020**, *836*, 155474. [CrossRef]
144. Kumar, N.; Mishra, A.; De, A.; Shankar, U.; Ranjan, R. Factors contributing to the local polar-structural heterogeneity and ultrahigh piezoelectricity in Sm-modified $Pb(Mg_{1/3}Nb_{2/3})O_3$–$PbTiO_3$. *J. Phys. D Appl. Phys.* **2020**, *53*, 165302. [CrossRef]
145. Li, Y.; Borbely, M.; Bell, A. The influence of oxygen vacancies on piezoelectricity in samarium-doped $Pb(Mg_{1/3}Nb_{2/3})O_3$-$PbTiO_3$ ceramics. *J. Am. Ceram. Soc.* **2021**, *104*, 2678–2688. [CrossRef]
146. Li, F.; Lin, D.; Chen, Z.; Cheng, Z.; Wang, J.; Li, C.; Xu, Z.; Huang, Q.; Liao, X.; Chen, L.Q.; et al. Ultrahigh piezoelectricity in ferroelectric ceramics by design. *Nat. Mater.* **2018**, *17*, 349–354. [CrossRef] [PubMed]
147. Guo, Q.; Meng, X.; Li, F.; Xia, F.; Wang, P.; Gao, X.; Wu, J.; Sun, H.; Hao, H.; Liu, H.; et al. Temperature-insensitive PMN-PZ-PT ferroelectric ceramics for actuator applications. *Acta Mater.* **2021**, *211*, 116871. [CrossRef]
148. Wang, P.; Guo, Q.; Li, F.; Xia, F.; Hao, H.; Sun, H.; Liu, H.; Zhang, S. Modified $Pb(Mg_{1/3}Nb_{2/3})O_3$-$PbZrO_3$–$PbTiO_3$ ceramics with high piezoelectricity and temperature stability. *J. Am. Ceram. Soc.* **2021**, *104*, 5127–5137. [CrossRef]
149. Guo, Q.; Li, F.; Xia, F.; Wang, P.; Gao, X.; Hao, H.; Liu, H.; Sun, H.; Zhang, S. Piezoelectric ceramics with high piezoelectricity and broad temperature usage range. *J. Mater.* **2021**, *7*, 683–692. [CrossRef]
150. Guo, Q.; Li, F.; Xia, F.; Gao, X.; Wang, P.; Hao, H.; Sun, H.; Liu, H.; Zhang, S. High-performance Sm-doped $Pb(Mg_{1/3}Nb_{2/3})O_3$-$PbZrO_3$–$PbTiO_3$-based piezoceramics. *ACS Appl. Mater. Interfaces* **2019**, *11*, 43359–43367. [CrossRef]
151. Li, F.; Zhang, S.; Damjanovic, D.; Chen, L.Q.; Shrout, T.R. Local structural heterogeneity and electromechanical responses of ferroelectrics: Learning from relaxor ferroelectrics. *Adv. Funct. Mater.* **2018**, *28*, 1801504. [CrossRef]
152. Li, C.; Xu, B.; Lin, D.; Zhang, S.; Bellaiche, L.; Shrout, T.R.; Li, F. Atomic-scale origin of ultrahigh piezoelectricity in samarium-doped PMN-PT ceramics. *Phys. Rev. B* **2020**, *101*, 140102. [CrossRef]
153. Srimathy, B.; Kumar, J. Effect of donor dopants on the properties of flux grown PZN-PT single crystals. *Appl. Phys. A* **2021**, *127*, 1–7. [CrossRef]
154. Davis, M.; Budimir, M.; Damjanovic, D.; Setter, N. Rotator and extender ferroelectrics: Importance of the shear coefficient to the piezoelectric properties of domain-engineered crystals and ceramics. *J. Appl. Phys.* **2007**, *101*, 054112. [CrossRef]

155. Jin, J.; Rajan, K.K.; Lim, L.C. Properties of single domain $Pb(Zn_{1/3}Nb_{2/3})O_3$–(6–7)%$PbTiO_3$ single crystal. *Jpn. J. Appl. Phys.* **2006**, *45*, 8744. [CrossRef]
156. Zhang, R.; Jiang, B.; Cao, W. Orientation dependence of piezoelectric properties of single domain $0.67Pb(Mn_{1/3}Nb_{2/3})O_3$–$0.33PbTiO_3$ crystals. *Appl. Phys. Lett.* **2003**, *82*, 3737–3739. [CrossRef]
157. Zhang, S.; Liu, G.; Jiang, W.; Luo, J.; Cao, W.; Shrout, T.R. Characterization of single domain $Pb(In_{0.5}Nb_{0.5})O_3$-$Pb(Mg_{1/3}Nb_{2/3})O_3$-$PbTiO_3$ crystals with monoclinic phase. *J. Appl. Phys.* **2011**, *110*, 064108. [CrossRef]
158. Sun, E.; Qi, X.; Cao, W.; Zhang, R.; Yang, B.; Zhao, L. Electromechanical properties of orthorhombic $0.24Pb(In_{1/2}Nb_{1/2})O_3$–$0.43Pb(Mg_{1/3}Nb_{2/3})O_3$–$0.33PbTiO_3$ single-domain crystal. *Mater. Lett.* **2015**, *157*, 163–165. [CrossRef] [PubMed]
159. Liu, X.; Zhang, S.; Luo, J.; Shrout, T.R.; Cao, W. A complete set of material properties of single domain $0.26Pb(In_{1/2}Nb_{1/2})O_3$–$0.46Pb(Mg_{1/3}Nb_{2/3})O_3$–$0.28PbTiO_3$ single crystals. *Appl. Phys. Lett.* **2010**, *96*, 012907. [CrossRef]
160. Damjanovic, D. A morphotropic phase boundary system based on polarization rotation and polarization extension. *Appl. Phys. Lett.* **2010**, *97*, 062906. [CrossRef]
161. Sun, E.; Cao, W.; Jiang, W.; Han, P. Complete set of material properties of single domain $0.24Pb(In_{1/2}Nb_{1/2})O_3$-$0.49Pb(Mg_{1/3}Nb_{2/3})O_3$-$0.27PbTiO_3$ single crystal and the orientation effects. *Appl. Phys. Lett.* **2011**, *99*, 032901. [CrossRef]
162. Han, P.; Yan, W.; Tian, J.; Huang, X.; Pan, H. Cut directions for the optimization of piezoelectric coefficients of lead magnesium niobate–lead titanate ferroelectric crystals. *Appl. Phys. Lett.* **2005**, *86*, 052902. [CrossRef]
163. Kuwata, J.; Uchino, K.; Nomura, S. Dielectric and piezoelectric properties of $0.91Pb(Zn_{1/3}Nb_{2/3})O_3$-$0.09PbTiO_3$ single crystals. *Jpn. J. Appl. Phys.* **1982**, *21*, 1298. [CrossRef]
164. Damjanovic, D.; Budimir, M.; Davis, M.; Setter, N. Monodomain versus polydomain piezoelectric response of $0.67P(Mg_{1/3}Nb_{2/3})O_3$–$0.33PbTiO_3$ single crystals along nonpolar directions. *Appl. Phys. Lett.* **2003**, *83*, 527–529. [CrossRef]
165. Luan, Z.; Jiang, G.; Wang, J.; Liu, D.; Yang, B.; Wu, F. The intrinsic and extrinsic contributions in [001] oriented (1-x)$Pb(Mg_{1/3}Nb_{2/3})O_3$-x$PbTiO_3$ crystals. *Ferroelectrics* **2019**, *548*, 26–33. [CrossRef]
166. Haun, M.J.; Furman, E.; Jang, S.J.; McKinstry, H.A.; Cross, L.E. Thermodynamic theory of $PbTiO_3$. *J. Appl. Phys.* **1987**, *62*, 3331–3338. [CrossRef]
167. Zgonik, M.; Bernasconi, P.; Duelli, M.; Schlesser, R.; Günter, P.; Garrett, M.H.; Rytz, D.; Zhu, Y.; Wu, X. Dielectric, elastic, piezoelectric, electro-optic, and elasto-optic tensors of $BaTiO_3$ crystals. *Phys. Rev. B* **1994**, *50*, 5941. [CrossRef]
168. Li, F.; Jin, L.; Xu, Z.; Zhang, S. Electrostrictive effect in ferroelectrics: An alternative approach to improve piezoelectricity. *Appl. Phys. Rev.* **2014**, *1*, 011103. [CrossRef]
169. Zhang, S.; Li, F.; Luo, J.; Xia, R.; Hackenberger, W.; Shrout, T.R. Investigation of single and multidomain $Pb(In_{0.5}Nb_{0.5})O_3$–$Pb(Mg_{1/3}Nb_{2/3})O_3$–$PbTiO_3$ crystals with mm 2 symmetry. *Appl. Phys. Lett.* **2010**, *97*, 132903. [CrossRef]
170. Zhang, S.; Laurent, L.; Liu, S.; Rhee, S.; Randall, C.A.; Shrout, T.R. Piezoelectric shear coefficients of $Pb(Zn_{1/3}Nb_{2/3})O_3$–$PbTiO_3$ single crystals. *Jpn. J. Appl. Phys.* **2002**, *41*, L1099. [CrossRef]
171. Zhang, S.; Jiang, W.; Meyer, R.J., Jr.; Li, F.; Luo, J.; Cao, W. Measurements of face shear properties in relaxor-$PbTiO_3$ single crystals. *J. Appl. Phys.* **2011**, *110*, 064106. [CrossRef]
172. Zhang, S.; Li, F.; Jiang, W.; Luo, J.; Meyer, R.J., Jr.; Cao, W.; Shrout, T.R. Face shear piezoelectric properties of relaxor-$PbTiO_3$ single crystals. *Appl. Phys. Lett.* **2011**, *98*, 182903. [CrossRef]
173. Zhou, Y.; Li, Q.; Xu, C.; Zhuo, F.; Liu, D.; Yan, Q.; Zhang, Y.; Chu, X. Anisotropic temperature–electric field phase diagrams and domain structure evolution in rhombohedral Mn-doped PIN–PMN–PT single crystals. *CrystEngComm* **2018**, *20*, 5169–5179. [CrossRef]
174. Fang, H.; Wang, L.; Kuai, W.; Du, J.; Jiang, G.; Lu, X.; Zhao, M.; Wang, C.; Su, W.; Zheng, L.; et al. Reversible and irreversible domain wall dynamics in $[011]_C$ oriented relaxor ferroelectric single crystals. *J. Am. Ceram. Soc.* **2020**, *103*, 3257–3264. [CrossRef]
175. Zhou, Y.; Li, Q.; Zhuo, F.; Xu, C.; Yan, Q.; Zhang, Y.; Chu, X. Domain switching and polarization fatigue in rhombohedral PIN-PMN-PT and Mn-doped PIN-PMN-PT single crystals. *J. Am. Ceram. Soc.* **2019**, *102*, 6668–6679. [CrossRef]
176. Thakre, A.; Kumar, A.; Jeong, D.Y.; Hwang, G.T.; Yoon, W.H.; Lee, H.Y.; Ryu, J. Enhanced mechanical quality factor of 32 mode Mn doped $71Pb(Mg_{1/3}Nb_{2/3})O_3$–$29PbZrTiO_3$ piezoelectric single crystals. *Electron. Mater. Lett.* **2020**, *16*, 156–163. [CrossRef]
177. Sherlock, N.P.; Garten, L.M.; Zhang, S.J.; Shrout, T.R.; Meyer, R.J., Jr. Nonlinear dielectric response in piezoelectric materials for underwater transducers. *J. Appl. Phys.* **2012**, *112*, 124108. [CrossRef]
178. Zheng, L.; Yang, L.; Li, Y.; Lu, X.; Huo, D.; Lü, W.; Zhang, R.; Yang, B.; Cao, W. Origin of improvement in mechanical quality factor in acceptor-doped relaxor-based ferroelectric single crystals. *Phys. Rev. Appl.* **2018**, *9*, 064028. [CrossRef]
179. Jing, Y.; Zheng, L.; Liu, F.; Qi, X.; Jiang, G.; Fan, J.; Liu, G.; Lü, W. A large and anisotropic enhancement of the mechanical quality factor in ternary relaxor-$PbTiO_3$ single crystals. *Appl. Phys. Lett.* **2021**, *118*, 182902. [CrossRef]
180. Sherlock, N.P. Relaxor-PT Single Crystals for Broad Bandwidth, High Power Sonar Projectors. Ph.D. Thesis, The Pennsylvania State University, University Park, PA, USA, 2010.
181. Meyer, R.J.; Montgomery, T.C.; Hughes, W.J. Tonpilz transducers designed using single crystal piezoelectrics. In Proceedings of the 2002 OCEANS'02 MTS/IEEE, Biloxi, MI, USA, 29–31 October 2002; pp. 2328–2333.
182. Thompson, S.C.; Meyer, R.J.; Markley, D.C. Performance of tonpilz transducers with segmented piezoelectric stacks using materials with high electromechanical coupling coefficient. *J. Acoust. Soc. Am.* **2014**, *135*, 155–164. [CrossRef] [PubMed]

183. Zhang, K.; Huang, D.; Chen, B.R.; Tang, Y.Z. Wideband Single Crystal Longitudinal Transducer for Underwater Sound. In Proceedings of the 2019 14th Symposium on Piezoelectricity, Acoustic Waves and Device Applications (SPAWDA), Shijiazhuang, China, 1–4 November 2019; pp. 1–3.
184. Sherlock, N.P.; Meyer, R.J. Modified single crystals for high-power underwater projectors. *IEEE Trans. Ultrason. Ferroelectr. Freq. Control* **2012**, *59*, 1285–1291. [CrossRef] [PubMed]
185. Guo, R.; Li, S.; An, D.; Han, T.; Chen, J.; Cao, W. Comprehensive analysis of Mn:PIN-PMN-PT single crystals for Class IV flextensional transducer. *Ceram. Int.* **2018**, *44*, 2864–2868. [CrossRef]
186. Zhou, Q.; Lam, K.H.; Zheng, H.; Qiu, W.; Shung, K.K. Piezoelectric single crystal ultrasonic transducers for biomedical applications. *Prog. Mater. Sci.* **2014**, *66*, 87–111. [CrossRef] [PubMed]
187. Lee, H.J.; Zhang, S.; Bar-Cohen, Y.; Sherrit, S. High temperature, high power piezoelectric composite transducers. *Sensor* **2014**, *14*, 14526–14552. [CrossRef] [PubMed]
188. Zhou, Q.; Wu, D.; Jin, J.; Hu, C.H.; Xu, X.; Williams, J.; Cannata, J.M.; Lim, L.; Shung, K.K. Design and fabrication of PZN-7%PT single crystal high frequency angled needle ultrasound transducers. *IEEE Trans. Ultrason. Ferroelectr. Freq. Control* **2008**, *55*, 1394–1399. [CrossRef] [PubMed]
189. Zhou, Q.; Xu, X.; Gottlieb, E.J.; Sun, L.; Cannata, J.M.; Ameri, H.; Humayun, M.S.; Han, P.; Shung, K.K. PMN-PT single crystal, high-frequency ultrasonic needle transducers for pulsed-wave Doppler application. *IEEE Trans. Ultrason. Ferroelectr. Freq. Control* **2007**, *54*, 668–675. [CrossRef]
190. Shung, K.K.; Cannata, J.M.; Zhou, Q.F. Piezoelectric materials for high frequency medical imaging applications: A review. *J. Electroceram.* **2007**, *19*, 141–147. [CrossRef]
191. Lam, K.H.; Chen, Y.; Cheung, K.F.; Dai, J.Y. PMN–PT single crystal focusing transducer fabricated using a mechanical dimpling technique. *Ultrasonics* **2012**, *52*, 20–24. [CrossRef]
192. Chen, Y.; Lam, K.H.; Zhou, D.; Cheng, W.F.; Dai, J.Y.; Luo, H.S.; Chan, H.L.W. High frequency PMN–PT single crystal focusing transducer fabricated by a mechanical dimpling technique. *Ultrasonics* **2013**, *53*, 345–349. [CrossRef]
193. Chen, Y.; Qiu, W.B.; Lam, K.H.; Liu, B.Q.; Jiang, X.P.; Zheng, H.R.; Luo, H.S.; Chan, H.L.W.; Dai, J.Y. Focused intravascular ultrasonic probe using dimpled transducer elements. *Ultrasonics* **2015**, *56*, 227–231. [CrossRef]
194. Fei, C.; Yang, Y.; Guo, F.; Lin, P.; Chen, Q.; Zhou, Q.; Sun, L. PMN-PT single crystal ultrasonic transducer with half-concave geometric design for IVUS imaging. *IEEE Trans. Biomed. Eng.* **2017**, *65*, 2087–2092. [CrossRef]
195. Jae Lee, H.; Zhang, S.; Meyer, R.J., Jr.; Sherlock, N.P.; Shrout, T.R. Characterization of piezoelectric ceramics and 1–3 composites for high power transducers. *Appl. Phys. Lett.* **2012**, *101*, 032902. [CrossRef]
196. Lee, H.J.; Zhang, S. Design of low-loss 1-3 piezoelectric composites for high-power transducer applications. *IEEE Trans. Ultrason. Ferroelectr. Freq. Control* **2012**, *59*, 1969–1975.
197. Wong, C.M.; Chen, Y.; Luo, H.; Dai, J.; Lam, K.H.; Chan, H.L.W. Development of a 20-MHz wide-bandwidth PMN-PT single crystal phased-array ultrasound transducer. *Ultrasonics* **2017**, *73*, 181–186. [CrossRef] [PubMed]
198. Zhou, D.; Chen, J.; Luo, H. Piezoelectric single crystals of $Pb(Mg_{1/3}Nb_{2/3})O_3$-$PbTiO_3$ and their applications in medical ultrasonic transducers. In Proceedings of the 2008 International Conference on BioMedical Engineering and Informatics, Sanya, China, 27–30 May 2008; pp. 662–666.
199. Zhou, D.; Cheung, K.F.; Chen, Y.; Lau, S.T.; Zhou, Q.; Shung, K.K.; Luo, H.S.; Dai, J.; Chan, H.L.W. Fabrication and performance of endoscopic ultrasound radial arrays based on PMN-PT single crystal/epoxy 1–3 composite. *IEEE Trans. Ultrason. Ferroelectr. Freq. Control* **2011**, *58*, 477–484. [CrossRef] [PubMed]
200. Lau, S.T.; Li, H.; Wong, K.S.; Zhou, Q.F.; Zhou, D.; Li, Y.C.; Luo, H.S.; Shung, K.K.; Dai, J.Y. Multiple matching scheme for broadband $0.72Pb(Mg_{1/3}Nb_{2/3})O_3-0.28PbTiO_3$ single crystal phased-array transducer. *J. Appl. Phys.* **2009**, *105*, 094908. [CrossRef] [PubMed]
201. Wang, J.; Chen, M.; Zhao, X.; Wang, F.; Tang, Y.; Lin, D.; Luo, H. Fabrication and high acoustic performance of high frequency needle ultrasound transducer with PMN-PT/Epoxy 1–3 piezoelectric composite prepared by dice and fill method. *Sens. Actuator A Phys.* **2021**, *318*, 112528. [CrossRef]
202. Yang, X.; Li, Z.; Fei, C.; Liu, Y.; Li, D.; Hou, S.; Zhang, L.; Li, F.; Yang, Y.; Zhou, Q.; et al. High frequency needle ultrasonic transducers based on Mn doped piezoelectric single crystal. *J. Alloys Compd.* **2020**, *832*, 154951. [CrossRef]
203. Lee, H.J.; Zhang, S.; Luo, J.; Li, F.; Shrout, T.R. Thickness-dependent properties of relaxor-$PbTiO_3$ ferroelectrics for ultrasonic transducers. *Adv. Funct. Mater.* **2010**, *20*, 3154–3162. [CrossRef] [PubMed]
204. Lee, H.J.; Zhang, S.; Shrout, T.R. Scaling effects of relaxor-$PbTiO_3$ crystals and composites for high frequency ultrasound. *J. Appl. Phys.* **2010**, *107*, 124107. [CrossRef]
205. Wan, H.; Kim, H.; Wu, H.; Luo, C.; Jiang, X. Characterization of high-frequency ultrasound transducers made of alternating current poled $Pb(Mg_{1/3}Nb_{2/3})O_3$-$xPbTiO_3$ single crystals. In Proceedings of the 2020 IEEE International Ultrasonics Symposium (IUS), Las Vegas, NV, USA, 7–11 September 2020; pp. 1–4.
206. Xu, J.; Zhang, Z.; Liu, S.; Xiao, J.; Yue, Q.; Deng, H.; Wang, X.; Lin, D.; Wang, F.; Zhang, R.; et al. Optimizing the piezoelectric vibration of $Pb(Mg_{1/3}Nb_{2/3})O_3$-$0.25PbTiO_3$ single crystal by alternating current polarization for ultrasonic transducer. *Appl. Phys. Lett.* **2020**, *116*, 202903. [CrossRef]
207. Qiu, C.; Liu, J.; Li, F.; Xu, Z. Thickness dependence of dielectric and piezoelectric properties for alternating current electric-field-poled relaxor-$PbTiO_3$ crystals. *J. Appl. Phys.* **2019**, *125*, 014102. [CrossRef]

208. Uchino, K. Electro-optic ceramics and their display applications. *Ceram. Int.* **1995**, *21*, 309–315. [CrossRef]
209. Zheng, L.; Jing, Y.; Lu, X.; Li, S.; Yang, L.; Lü, W.; Cao, W. Temperature dependent piezoelectric anisotropy in tetragonal 0.63Pb($Mg_{1/3}Nb_{2/3}$)-0.37$PbTiO_3$ single crystal. *Appl. Phys. Lett.* **2018**, *113*, 102903. [CrossRef]
210. Li, F.; Zhang, S.; Lin, D.; Luo, J.; Xu, Z.; Wei, X.; Shrout, T.R. Electromechanical properties of Pb($In_{1/2}Nb_{1/2}$)O_3–Pb($Mg_{1/3}Nb_{2/3}$)O_3–$PbTiO_3$ single crystals. *J. Appl. Phys.* **2011**, *109*, 014108. [CrossRef]
211. Lin, D.; Lee, H.J.; Zhang, S.; Li, F.; Li, Z.; Xu, Z.; Shrout, T.R. Influence of domain size on the scaling effects Pb($Mg_{1/3}Nb_{2/3}$)O_3-$PbTiO_3$ ferroelectric crystals. *Scr. Mater.* **2011**, *64*, 1149–1151. [CrossRef]
212. Li, F.; Zhang, S.; Luo, J.; Geng, X.; Xu, Z.; Shrout, T.R. [111]-oriented PIN-PMN-PT crystals with ultrahigh dielectric permittivity and high frequency constant for high-frequency transducer applications. *J. Appl. Phys.* **2016**, *120*, 074105. [CrossRef]
213. Lebrun, L.; Sebald, G.; Guiffard, B.; Richard, C.; Guyomar, D.; Pleska, E. Investigations on ferroelectric PMN–PT and PZN–PT single crystals ability for power or resonant actuators. *Ultrasonics* **2004**, *42*, 501–505. [CrossRef]
214. Hou, X.Y.; Lee, H.P.; Lim, S.P.; Ong, C.J. Performance enhancement of ultrasonic motors using single crystalline piezo-materials. In Proceedings of the 2012 Digest APMRC, Singapore, 31 October–2 November 2012; pp. 1–2.
215. Li, S.; Jiang, W.; Zheng, L.; Cao, W. A face-shear mode single crystal ultrasonic motor. *Appl. Phys. Lett.* **2013**, *102*, 183512. [CrossRef]
216. Ci, P.; Liu, G.; Chen, Z.; Zhang, S.; Dong, S. High-order face-shear modes of relaxor-$PbTiO_3$ crystals for piezoelectric motor applications. *Appl. Phys. Lett.* **2014**, *104*, 242911. [CrossRef]
217. Ou, W.; Li, S.; Cao, W.; Yang, M. A single-mode Mn-doped 0.27PIN-0.46PMN-0.27PT single-crystal ultrasonic motor. *J. Electroceram.* **2016**, *37*, 121–126. [CrossRef]